J. Fluid Mech. (2002), *vol.* 462, *pp.* 209–243.
DOI: 10.1017/S0022112002008650 Printed in the United Kingdom

Anisotropic enhancement of turbulence in large-scale, low-intensity turbulent premixed propane–air flames

By JUNICHI FURUKAWA[1], YOSHIKI NOGUCHI[2], TOSHISUKE HIRANO[3] AND FORMAN A. WILLIAMS[4]

[1]Department of Mechanical Engineering, Tokyo Metropolitan College of Technology, 1-10-40 Higashi-Ohi, Shinagawa-Ku, Tokyo 140-0011, Japan
furukawa@tokyo-tmct.ac.jp

[2]Department of Mechanical Engineering, Sophia University, 7 Kioicho, Chiyoda-Ku, Tokyo 102-8554, Japan

[3]Department of Chemical System Engineering, University of Tokyo, 7-3-1 Hongo, Bunkyo-Ku, Tokyo 113-8656, Japan

[4]Department of Mechanical and Aerospace Engineering, University of California, San Diego, La Jolla, CA 92093-0411, USA

(Received 20 August 2001 and in revised form 22 January 2002)

The density change across premixed flames propagating in turbulent flows modifies the turbulence. The nature of that modification depends on the regime of turbulent combustion, the burner design, the orientation of the turbulent flame and the position within the flame. The present study addresses statistically stationary turbulent combustion in the flame-sheet regime, in which the laminar-flame thickness is less than the Kolmogorov scale, for flames stabilized on a vertically oriented cylindrical burner having fully developed upward turbulent pipe flow upstream from the exit. Under these conditions, rapidly moving wrinkled laminar flamelets form the axisymmetric turbulent flame brush that is attached to the burner exit. Predictions have been made of changes in turbulence properties across laminar flamelets in such situations, but very few measurements have been performed to test the predictions. The present work measures individual velocity changes and changes in turbulence across flamelets at different positions in the turbulent flame brush for three different equivalence ratios, for comparison with theory.

The measurements employ a three-element electrostatic probe (EP) and a two-component laser-Doppler velocimeter (LDV). The LDV measures axial and radial components of the local gas velocity, while the EP, whose three sensors are located in a vertical plane that passes through the burner axis, containing the plane of the LDV velocity components, measures arrival times of flamelets at three points in that plane. From the arrival times, the projection of flamelet orientation and velocity on the plane are obtained. All of the EP and LDV sensors are located within a fixed volume element of about 1 mm diameter to provide local, time-resolved information. The technique has the EP advantages of rapid response and good sensitivity and the EP disadvantages of intrusiveness and complexity of interpretation, but it is well suited to the type of data sought here.

Theory predicts that the component of velocity tangent to the surface of a locally planar flamelet remains constant in passing through the flamelet. The data are consistent with this prediction, within the accuracy of the measurement. The data also indicate that the component of velocity normal to the flamelet, measured with respect to the flamelet, tends to increase in passing through the flamelet, as expected.

The flamelets thereby can generate anisotropy in initially isotropic turbulence. They also produce differences in turbulent spectra conditioned on unburnt or burnt gas. Local modifications of turbulence by flamelets thus are demonstrated experimentally. The modifications are quantitatively different at different locations in the turbulent flame brush but qualitatively similar in that the turbulence is enhanced more strongly in the radial direction than in the axial direction at all positions in these flames.

1. Introduction

Premixed turbulent combustion exhibits a wide variety of phenomena that differ in different regimes. Damköhler (1940) was the first to identify two limiting regimes, one in which the laminar deflagration thickness is small compared with all turbulence scales and the other in which all turbulence scales are small compared with the laminar deflagration thickness. These two limits are flame-sheet and distributed-reaction limits, corresponding to large and small Damköhler numbers, respectively, in figure 1. The Damköhler number on the ordinate of this figure is Damköhler's first similarity group (Damköhler 1936), the ratio of a flow time to a chemical time, in this case the flow time being the large-eddy turnover time of the turbulence and the chemical time the transit time of a fluid element through a laminar deflagration. Notations appearing in figure 1 are K_L, the turbulent kinetic energy referred to the (laminar) ratio of kinematic viscosity to chemical time, D_K, the Damköhler first similarity group based on the Kolmogorov time scale instead of the integral time scale, and L_D, the ratio of the integral length scale to the thickness of a laminar deflagration. The present contribution pertains to large Damköhler numbers, the top part of figure 1.

The lines of constant values of the three additional parameters (K_L, D_K and L_D) in figure 1 serve to further divide conditions into subregimes. For example, the line $K_L = 1$ divides the flame-sheet regime into single-sheet and multiple-sheet regimes. The present experiments lie near this boundary ($K_L = 1$), at turbulence Reynolds numbers between 100 and 500, in the general region of the circle shown in the figure.

Other diagrams that are equivalent to figure 1 can be constructed by selecting different lines in figure 1 as axes for the ordinate and abscissa. For example, the popular Borghi diagram (Borghi 1985; Peters 2000) employs $L_D = 1$ as the ordinate, with $\sqrt{K_L}$ as the axis increasing vertically, and $K_L = 1$ as the abscissa, with L_D as the axis increasing horizontally. Much of the literature citing this last diagram calls the multiple-sheet regime the corrugated-flamelet regime and the single-sheet regime the wrinkled-flamelet regime, with the idea that corrugations are more pronounced than wrinkles. In that terminology, then, the present experiments lie near the boundary of the corrugated-flamelet and wrinkled-flamelet regimes.

The single-sheet regime in figure 1 has small values of the ratio of the root-mean-square turbulent velocity fluctuations to the laminar deflagration velocity (a ratio proportional to $\sqrt{K_L}$) so that turbulence does not wrinkle the flame sheet strongly, whereas the multiple-sheet regime has large values of this ratio, leading to large influences of turbulent convection on the shape of the flame sheet, many folds in the sheet, formation of pockets of unburnt gas at sufficiently large Reynolds numbers and a very irregularly shaped flame sheet, reasoned (Kerstein 1988; Joulin 1999) to be fractal with a fractal dimension of $2\frac{1}{3}$ at large Reynolds numbers, over a size range between the integral length scale and the Gibson length scale (Peters 1986, 2000), the ratio of the cube of the laminar deflagration velocity to the average rate of dissipation

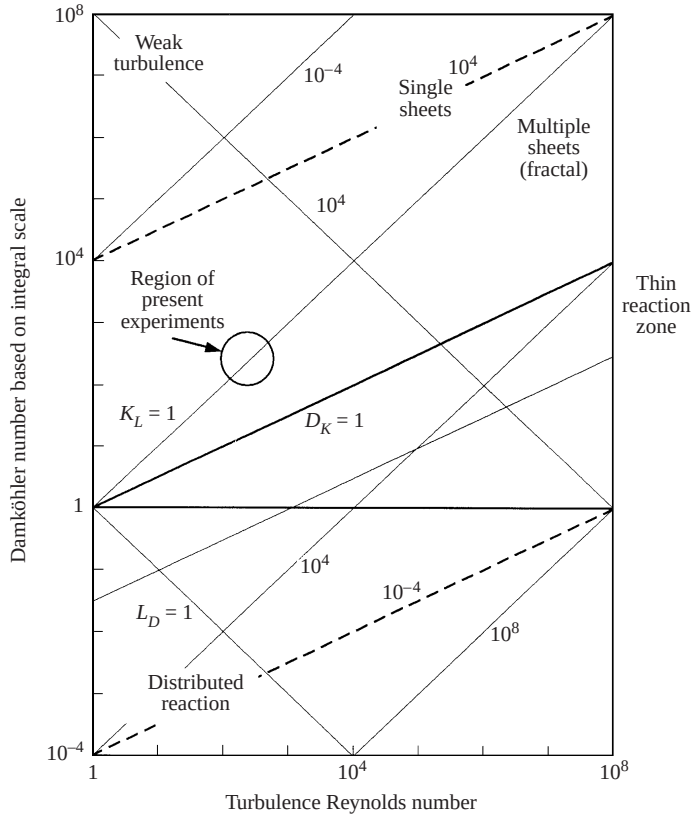

FIGURE 1. Diagram of regimes of turbulent flame propagation, showing different flame classifications. The circle identifies location of present experiments.

of turbulent kinetic energy. A new regime has been identified recently (Peters 1999, 2000), the thin-reaction-zone regime indicated in figure 1, in which turbulence scales are smaller than the deflagration thickness, but the reaction zone, always thinner than the deflagration, is smaller than turbulence scales, remaining intact, although highly wrinkled, as the turbulence modifies the preheat zone internally. The present experiments are well removed from this regime and never far enough into the multiple-sheet regime for fractal descriptions to be very useful.

Flames modify turbulence in many ways. In all of the regimes of figure 1, the large temperature increase at nearly constant pressure increases the kinematic viscosity by more than an order of magnitude, thereby decreasing turbulence Reynolds numbers, often substantially, tending to accelerate relaminarization. An additional general influence, associated with the density decreases produced by the temperature increase, is that turbulence scales are anticipated to tend to be larger in the product stream as a consequence of the expansion of the volume per unit mass. In the flame-sheet regimes of the present experiments, the density decrease across the sheet mechanistically modifies turbulence locally as well. Karlovitz (1953, 1956) was the first to popularize 'flame-generated turbulence' by observing that since the accepted jump conditions require continuity of velocity components tangential to a sheet and an increase in the velocity component normal to a sheet in a frame of reference moving locally with the sheet, turbulent velocity fluctuations with respect to the sheets are augmented by the flamelets. The specific manner in which these jump conditions modify turbulence

depends on the configuration and is not fully understood in every case, notably in the multiple-sheet regime. Clavin & Williams (1982) concluded that for large-scale, low-intensity turbulence the enhancement in turbulent kinetic energy initially occurs in velocity components transverse to the flame, but Aldredge & Williams (1991) found that at low turbulence intensities in planar, one-dimensional, flat-flame configurations, there is a downstream region of hydrodynamic adjustment with thickness of the order of the integral scale, across which the transverse fluctuations are transformed into mainly longitudinal fluctuations, so that the enhancement ultimately appears preferentially in the normal direction. An objective of the present study is to investigate how flamelets modify turbulence in non-planar burner-stabilized flames having turbulence intensities too large for reliable application of perturbation analyses like those employed in these two studies.

Two types of experimental result are reported here. First, local, instantaneous information is given on flamelet position, velocity and orientation and on gas velocity vectors ahead of and behind the flamelet. This information allows testing of jump conditions across individual flamelets within the turbulent flame brush. Prior to the present program, experimental verifications of jump conditions have been made only for steady laminar flames (Lewis & von Elbe 1987). The turbulent results are obtained by coordinated measurements with a three-element electrostatic probe (EP) and a two-component laser-Doppler velocimeter (LDV). Although similar data could be generated, in principle, by simultaneous use of sufficiently highly time-resolved and space-resolved planar laser-induced fluorescence, for example, in conjunction with either LDV or PIV (particle-image velocimetry) techniques, such non-intrusive methods are not yet well enough developed to have provided this detailed information.

The second type of result concerns statistically averaged quantities. Turbulent kinetic-energy spectra, in particular, conditioned on being in either unburnt or burnt gas, are derived from the LDV data, with the conditioning provided by the EP signal. Previously reported spectra for premixed turbulent flames are scarce, are seldom conditioned and mainly concern scalar fields. Gökalp, Shepherd & Cheng (1988) report conditioned kinetic-energy spectra for wire-stabilized V-flames, obtained from a one-component LDV with Rayleigh-scattering conditioning. Videto & Santavicca (1990) obtained similarly conditioned kinetic-energy spectra by the same general methods (but with a two-component LDV) for a planar turbulent flame freely propagating downward in an upward mean flow. Through comparisons with these earlier results, dependences of spectra on specific configurations will be emphasized in the present work.

All of the measurements reported here are two-dimensional, made in a vertical plane that passes through the axis of the burner. Three-dimensional behaviour can call into question some types of EP result. It will be demonstrated below that, for the type of data acquired in the present study, three-dimensional effects do not introduce difficulties. The measurements are thus considered reliable for the flames and configuration investigated, in providing certain jump conditions and certain measures of turbulence effects.

Furukawa, Noguchi & Hirano (2000) report these same types of measurement at one position in one of the flames studied here. Measurements were performed at a number of different positions in the present work, allowing some new conclusions to be drawn concerning spatial dependences for the flame investigated by Furukawa *et al.* (2000), and measurements were also made on different propane–air flames, producing conclusions on influences of equivalence ratios. A further important contribution of

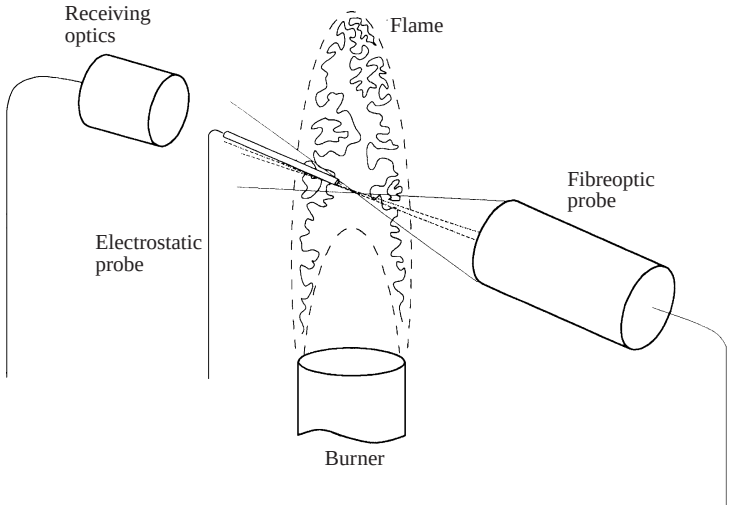

FIGURE 2. Schematic illustration of the experimental arrangement.

the present paper concerns the detailed consideration of the reliability, accuracy and meaning of the results and their implications for future research.

After an explanation of the principles of the measurements, the limitations of the EP and LDV and associated error analyses are addressed. Results concerning flamelet jump conditions are then presented, followed by statistical results including conditioned spectra of turbulent kinetic energy. Finally, the conclusions that can be drawn from this study and prospects for future work are discussed.

2. The principles of the measurements

The objective is to make measurements at a fixed point in the laboratory frame, for a turbulent flame statistically stationary in that frame. Simultaneous information is sought on both gas and flamelet motion, the former by the LDV and the latter by the EP. Figure 2 is a schematic illustration of the experimental arrangement. It will be helpful to state first specific details of the LDV and EP measurements that were made here.

The LDV employed a 1.0 W argon ion laser, operating with multiple lines in a two-colour, four-beam, forward-scattering optical arrangement, with a TSI IFA-750 Doppler signal analyser. The horizontal fibreoptic probe focused the beam at a point in a plane passing through the vertical burner axis. The split beams intersected at a narrow angle, producing an approximately prolate-spheroidally shaped intersection region of 0.11 mm in diameter in the measurement plane and 1.60 mm long, normal to the plane, as measured optically from light scattered by fog. This measured diameter is indicative of the diameter of the measurement volume, but its length, on average, will be less than 1.60 mm because of the low probability of seeding particles being detected at the narrow points on the extremes of the volume. The seeding density of submicron particles of SiO_2 powder was adjusted to provide sampling rates of 20 kHz in the burnt gas, giving higher sampling rates elsewhere, so that average sampling rates were of the order of 40 kHz (Furukawa, Okamoto & Hirano 1996). Accuracies of resulting samples of radial and axial velocity components are comparable with

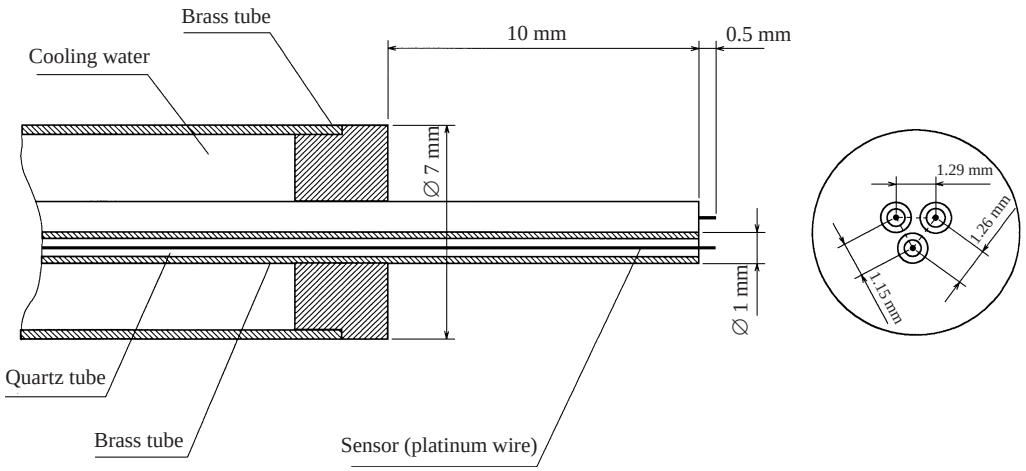

FIGURE 3. Illustration of the design of the electrostatic probe.

expectations from previous LDV measurements in flames and are discussed in the following section.

The EPs applied in the present study were of the same type as that employed by Furukawa, Hirano & Williams (1998*a*) and had three identical sensors, about 1 mm apart, in an equilateral triangular array, as illustrated in figure 3. The probe dimensions were measured microscopically after assembly. Each sensor was constructed from a platinum wire 0.1 mm in diameter with a 0.5 mm long exposed tip, projecting from a finely drawn, electrically insulating quartz tube about 0.3 mm in outer diameter. All three sensors had parallel leads, fitted for cooling purposes into a common water-cooled brass tube of 6 mm outer diameter, recessed about 10 mm and inserted into the flame nearly coaxially with the LDV receiving optics, as illustrated in figure 2. The centres of the exposed probe tips were placed coplanar with the centre of the vertical measurement plane of the LDV, and the EP was slightly above the LDV axis, with its two highest sensors each at the same elevation and its lowest sensor 0.5 mm above the centre of the LDV measurement volume, to facilitate acquisition of LDV data by avoiding interference from the EP. Each probe tip is maintained at −12 V with respect to the burner port. Each probe current is monitored by a separate parallel 10-bit analogue-to-digital (A/D) converter having a buffer memory of 256 K words, operated simultaneously from a common clock with a sampling frequency of 250 kHz, much lower than the 16 MHz capability of the converter, and selected to provide less than 3% error in measured arrival times. The analogue EP signals and the discrete LDV signals are thus both recorded digitally, but the EP sampling rate is much faster than the LDV sample acquisition rate. Both types of measurement are seen to be centred in the same vertical plane, having a measurement-volume diameter and depth each somewhat greater than 1 mm but much less than 2 mm.

The measurements are interpreted under the assumption that each flamelet is planar on the scale of this measurement volume. The accuracy of this assumption is addressed in the following section, where the EP capabilities, limitations and history are reviewed. For planar flamelets, the relevant EP data are the arrival times of the flamelet at each sensor. For locally planar flamelets, Furukawa *et al.* (1999) emphasized the desirability of making measurements with a 3-component LDV and a 4-element EP having tetrahedrally arranged elements. Such results ideally would provide all three velocity components of the gas and the complete orientation and velocity of

the flamelet. It then becomes possible, in principle, to determine all components of gas velocities with respect to each flamelet. Measurements of this kind are, however, very difficult to perform well, not only because of the complexity and expense of the 3-component LDV but also because of probe-interference effects of the intrusive EP. These effects, discussed in the following section, increase with the number of EP elements and can be quite severe with 4 elements. The ideal of obtaining complete velocity information therefore is not sought in the present work. Emphasis instead is placed on acquiring partial but unambiguous conclusions that can be drawn without complete velocity information.

Consider a planar flamelet that passes all three EP sensors and for which LDV data are obtained both before and after this passage. Typically, there are of the order of 10 LDV data points during such a flamelet-passage event, and the 'before' and 'after' data can be identified from the experimental traces, as illustrated in figure 4. These data give the gas velocity components in the vertical plane just before and after flamelet passage. The flamelet arrival times at each of the three EP sensors, obtained from the ion-current peaks that coincide approximately with the centre of the main reaction zone, provide the orientation of the line of intersection between the flamelet and the vertical plane and the projection of the flamelet motion vector into that plane. From the orientation of the line of intersection, the gas velocities can be resolved into components perpendicular and parallel to the intersection. If the tangential velocity is continuous across the flamelet, then the components of gas velocity parallel to the line of intersection must be the same before and after flamelet passage, since they are merely the projection of the full tangential velocity components into the vertical plane. Interpretation of the perpendicular components of gas velocity is more complicated because of the influences of the flamelet orientation and motion on the velocity of the line of intersection and on determining the extent to which the perpendicular gas velocity component is actually normal to the flamelet, but nevertheless an increase in gas velocity normal to the flamelet in crossing the flamelet will always be reflected in a larger perpendicular gas component after flamelet passage.

3. Aspects of the instrumentation and accuracy of measurement

Figure 4 shows representative LDV and EP traces. The LDV points exhibit a generally closer spacing of data in the fresh mixture than in the burnt gas as a consequence of the lower density of the reaction products. It is nevertheless possible to adjust the seeding so that reasonable data rates are obtained in both regions, as figure 4 indicates. There can be interference between the LDV and the EP in that the ion current in the burnt gas is observed to increase with increasing seeding density. This increase theoretically moves the ion-current maximum to a later time, but experimental seeding densities were kept low enough for this effect to remain entirely negligible in the present experiments. In addition, measurements on laminar flames at the seeding densities employed experimentally confirmed that the seeding had no observable effect on the laminar burning velocity. Point-to-point fluctuations of the LDV readings are observed in figure 4. These are associated with turbulent eddies, passage times of which are estimated to range from values on the order of 0.1 ms for Kolmogorov eddies to 5 ms for the largest eddies. Uncertainties in individual LDV data points, of the order of a few per cent, are generally small compared with these fluctuation. Because of the fluctuations, there is uncertainty in identifying gas velocities just before and just after flamelet passage. Accuracies no better than 10% result from this effect, possible errors sometimes being as large as 40%.

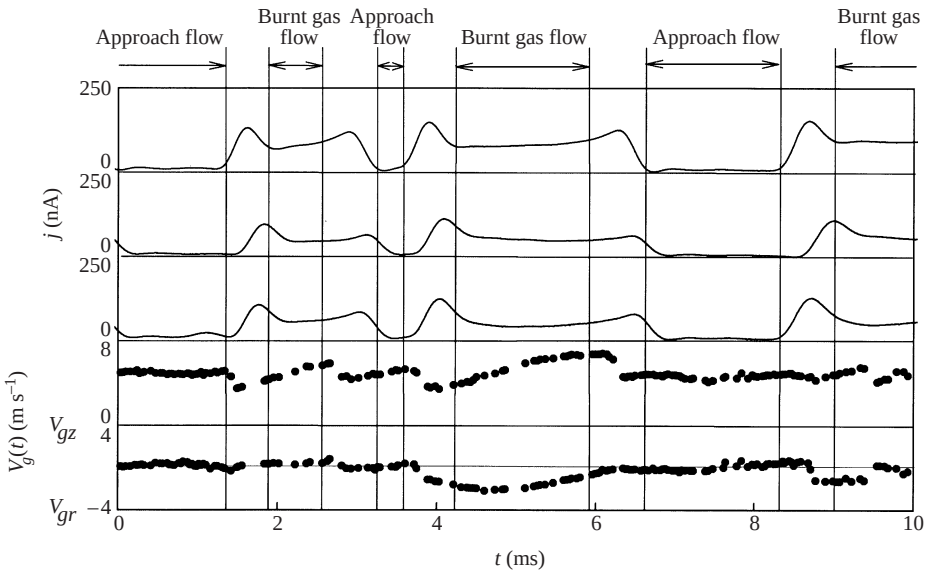

FIGURE 4. Typical traces of ion currents and velocity fluctuations.

The EP sensors have a long history of development, dating back to Langmuir (1923). In such devices, often called Langmuir probes, the negative potential repels electrons, so that the measured current is an ion current, proportional to the exposed probe surface area, the local ion number density and the random thermal velocities of ions in the region of free-molecule flow adjacent to the probe surface. During practical measurements in combustion gases, this current is controlled by the rate of ion diffusion through the boundary layer adjacent to the probe, ideally proportional to the ion number density outside the boundary layer and established in a time scale of the order of intermolecular collision times. The EP thus effectively responds to the local, instantaneous ion density in the flame, which is a maximum in the main reaction zone, where ions are produced by finite-rate chemical-kinetic processes during combustion. Neither the details of these production processes nor the maximum magnitude of the ion current need be understood well for most contemporary EP applications, in which the objectives are only to detect flame presence, flame passage and flame shape.

The EP literature is so large that it would be impractical to present a complete review of it here. Although originally applied to strongly ionized low-pressure plasmas, the EP in combustion measurements operates under weakly ionized high-pressure conditions even in the reaction zones. Probe theory under such conditions is considerably more complex (Lam 1964); the paper of Hirano (1972) may be consulted for a representative analysis and for entry into the literature. The ion diffusion through the boundary layer is ambipolar diffusion, electrical neutrality nearly being maintained until reaching a very thin sheath at the electrode. Complexities of the operation prevent theory from being applied directly in a quantitative manner, especially in flames, where the ions themselves are controlled by poorly understood finite-rate chemistry (Fialkov 1997). This does not negate the usefulness of the EP in flames, where its fine sensitivity and excellent spatial and temporal resolution are beneficial. It does, however, necessitate empirical determination of probe-response characteristics for extraction of most of the quantitative information. Many relevant measurements

of EP responses in flames have now been completed. It is helpful to review here the EP response characteristics that are most useful for measurements in turbulent combustion.

Many studies, dating back to Karlovitz *et al.* (1953), applied EP techniques to experiments on premixed turbulent flames. For the most part, the probes were used only to detect flame presence, based on peak ion current. Details of the probe response need not be known in such studies; it is sufficient to identify peak current with flame presence. Some studies were concerned with flame passage between two fixed points (Suzuki, Hirano & Tsuji 1978; Ventura *et al.* 1981). These measurements require two EP sensors, one at each point. The passage time is the time delay between the peak ion current of the two sensors. The EP characteristics enable not only the passage time to be measured but also the direction of passage to be determined, that is, whether the passage is from burnt to unburnt gas or from unburnt to burnt. It is clear from figure 4, for example, that the ion current is much lower in the fresh mixture than in the burnt gas. The direction of passage therefore is obtained merely by observing whether the peak follows or precedes in time the lower-current condition. This type of discrimination can, of course, be made even with a single sensor, but to obtain any information about the direction in space of the passage, at least two sensors are needed.

More ambitious studies require the use of ion-current histories during a single flame passage for interpreting results. Many such investigations were concerned with measuring ion densities and are not addressed here. Some were designed for use in measuring flamelet orientation or flamelet curvature. An inclined flat flame passing a probe produces a different ion-current history from a flame passing normal to the probe axis. Similarly, a curved flame has a different ion-current history from a flat flame in the same combustible mixture. Suzuki *et al.* (1979) mechanically passed an EP through steady laminar conical premixed flames on round burners of different radii at different distances from the centreline to catalogue the response as a function of the flame radius, probe velocity and position for later use in turbulent-flame measurements. Instead of using such catalogues for single probes, it is possible to employ data on influences of flame orientation (Furukawa, Harada & Hirano 1990; Furukawa *et al.* 1993*a*) to interpret two-sensor EP signals for extracting flamelet radii in turbulent flames (Furukawa *et al.* 1993; Furukawa, Nakamura & Hirano 1994; Furukawa & Hirano 1994). Results of such measurements for the main flames and configurations investigated in the present study yield a distribution of flame radii from about 1 mm to 10 mm, the average being about 4 mm for flamelets convex towards the unburnt mixture (Furukawa 1998*b*). These results are relevant to the interpretation of the present measurements, as discussed below.

The studies addressed thus far employed no more than two sensor elements in an EP. Although Travers & Williams (1965) considered three elements with floating potentials for measuring ion densities, Suzuki & Hirano (1984) were the first to employ three grounded elements for measuring projections of flamelet motion and orientation into the plane defined by the three sensors. Under the assumption that the flamelets are locally planar, their arrival times (as revealed by peak ion currents) and directions (fresh-to-burnt, or vice versa, as revealed by whether the lower voltage occurs before or after passage) provide the desired information, without the necessity of quantitative use of details of ion-current profiles during flamelet passage. Suzuki *et al.* (1986) added one-component LDV measurements to this to obtain information on movement relative to the gas. Our later studies with a three-element EP and a two-component LDV, such as that reported here, are outgrowths of this earlier work.

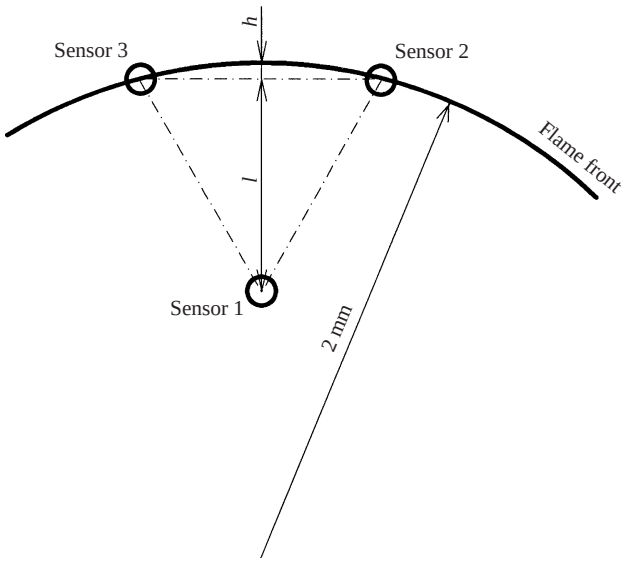

FIGURE 5. Illustration of errors associated with a curved flame passing the three sensors.

Since flamelets are curved, there are errors associated with interpretations of EP measurements that treat flamelets as flat. Even neglecting influences of flamelet curvature on flamelet burning velocity, there will be errors in measured flamelet transit times resulting from flamelet curvature. As a worst-case scenario, consider a curved flamelet propagating at constant velocity with its surface locally parallel to a line connecting two elements of a triangular three-element array, as illustrated in figure 5. The curvature introduces a fractional error in the elapsed arrival time equal to the ratio of the maximum distance between a circle passing through two sensors and a straight-line chord connecting the two sensors, the distance h in figure 5, to the distance between the third sensor and the chord, the distance l in figure 5. For the 1 mm sensor spacing of the present experiments and the 4 mm average flamelet radius indicated previously, this error is only 2%. There are, of course, flamelets with larger radii, which will have smaller errors than this average, and those with smaller radii, with errors approaching 10% at a 2 mm radius, seen in the figure. Small-radii effects become more dominant at the flamelet cusps. The present experiments, however, analyse only events detected by all three sensors, which are more likely to occur for larger flamelet radii since smaller flamelets would be less likely to encounter all the sensors; therefore geometrical errors are estimated not to exceed 5–10%. Similarly, curvature-induced changes in laminar burning velocities, of the order of the ratio of the laminar flame thickness to the radius of curvature, are estimated from the curvatures reported by Furukawa *et al.* (1998*b*) to be less than 10% for the flamelets measured. Total errors in interpretations associated with flamelet curvature, therefore, are estimated to be about 10%.

Errors associated with the intrusive character of the EP must also be considered. Even with a single sensor, a flamelet that travels along the sensor support is likely to experience an altered sensor response. With multiple sensors there is the further possibility of a flamelet being modified by one sensor before it reaches another. When the EP is combined with the LDV, an additional concern is that the probe may affect the measured velocity field. The separation between the LDV and EP measurement

points is selected in an effort to reduce this interference, and EP modifications of velocity fields are expected to have larger influences on EP sensor responses than on LDV data. These probe influences depend on the probe design (figure 3). In general, the greater the distance that the cooling and support tube is recessed from the sensor element, the less is the interference, but the sensors do not survive the flame with recess distances greater than 15–20 mm. The recess distances (10–13 mm) of the probes employed in the present work are a compromise that provides excellent robustness without excessive interference. Tests in which the LDV was employed for velocity measurements, with and without the probe present, indicated only small probe influences for velocity components or flamelet motion in the plane defined by the three EP sensor tips, that is, for flamelets that encounter the probe support axis broadside. For flamelets moving along the probe axis, however, interference effects can be substantial and alter arrival times, estimated, in the absence of any good way to make a quantitative measurement, to be 30% or more. Such events are rare and usually would produce signals deemed inappropriate for data reduction. Although quantitative error estimates are difficult to justify, it was judged that, on average, 5% of the uncertainties in arrival times arise from probe-interference effects in the data selected for detailed evaluation. Two-sensor results reported by Furukawa & Hirano (1994), who measured the small differences in instantaneous signals recorded by two identical EPs in turbulent flames, support this estimate.

The descretization of the EP signals introduces an additional error in arrival times. Figure 4 suggests that this error is not significant. Nevertheless, a detailed error analysis was performed, and it was found that at the sampling rate employed, this error was less than 2%. Combining this error with the errors estimated to arise from flamelet curvature and probe interference, the final total error estimates are 15% or less.

A further concern is that, to obtain data suitable for detailed analysis, a flamelet must be detected by all three EP sensors, and LDV data must be available both before and after, as previously indicated. A velocity signal is obtained when a seeding particle passes the measuring volume of the LDV. Three ion currents are obtained when a flamelet passes all three sensors of the electrostatic probe. The former measurement provides about 20 000 signals per second and the latter about 600 arrivals per second. However, the possibility that these two phenomena happen at the same time is low, so that only about 2% of the flame arrivals provide traces that can be used to extract data for the analysis in the following section. It may therefore be felt that only rare events are measured and that these events are not representative of most of the flamelets. Although there certainly is some selection, for example in excluding flamelets travelling along the probe support, it seems likely that the flamelets measured for the most part are representative and that the low probability of obtaining data is a consequence only of the number of conditions that must be satisfied and the random fluctuations of flamelets in the turbulent flame brush preventing all of these conditions from being satisfied very often. The selection therefore does not necessarily produce biasing of any significance. Moreover, with the objective of the detailed measurements restricted to testing jump conditions, there is no need to try to measure all possible flamelets. It is sufficient to acquire data wherever they can be secured.

4. Tests of flamelet jump conditions

The turbulent flame for which the jump conditions were tested most thoroughly was a slightly fuel-rich propane–air flame of equivalence ratio 1.10 on a cylindrical burner

Equivalence ratio	1.10		0.80, 1.40	
Burning velocity	$0.41\,\mathrm{m\,s^{-1}}$		$0.27\,\mathrm{m\,s^{-1}}$	
Measuring point	Centreline	Off-axis	Centreline	Off-axis
radius, height (mm)	$r = 0$, $z = 48$	$r = 9$, $z = 24$	$r = 0$, $z = 64$	$r = 10$, $z = 32$
Average velocity	$4.5\,\mathrm{m\,s^{-1}}$	$3.9\,\mathrm{m\,s^{-1}}$	$4.5\,\mathrm{m\,s^{-1}}$	$3.7\,\mathrm{m\,s^{-1}}$
Turbulence intensity	$0.22\,\mathrm{m\,s^{-1}}$	$0.38\,\mathrm{m\,s^{-1}}$	$0.22\,\mathrm{m\,s^{-1}}$	$0.41\,\mathrm{m\,s^{-1}}$
Integral scale	10.9 mm	12.9 mm	10.9 mm	13.7 mm
Taylor scale	3.5 mm	2.3 mm	3.5 mm	2.0 mm
Kolmogorov scale	260 μm	160 μm	260 μm	140 μm
Turbulence Reynolds number	154	314	154	360
Damköhler number	442	303	202	137

TABLE 1. Summary of experimental conditions of measurements for a cylindrical burner (26 mm diameter) with propane as the fuel at Reynolds number 6670.

26 mm in diameter with an average exit velocity (volume flow rate divided by exit area) of $4.0\,\mathrm{m\,s^{-1}}$, corresponding to fully developed pipe flow at a Reynolds number of about 7000, as summarized in table 1. The laminar burning velocity for this mixture is $0.41\,\mathrm{m\,s^{-1}}$ in the unburnt gas (Egolfopoulos & Vagelopoulos 1998) and about $3.2\,\mathrm{m\,s^{-1}}$ in the burnt gas, the maximum for any equivalence ratio, and the laminar flame thickness is of the order of 0.1 mm, the precise value depending on the specific definition employed. Measurements were also made on flames having equivalence ratios of 0.80 and 1.40, these lean and rich mixtures, respectively, having been selected to have approximately equal burning velocities for purposes of comparison, as indicated in table 1. Hot-wire measurements in cold flow with a single horizontal wire 5 μm in diameter registered root-mean-square velocity fluctuations having a peak off-axis value of $0.7\,\mathrm{m\,s^{-1}}$ and a centreline value of $0.2\,\mathrm{m\,s^{-1}}$ at the burner exit, as seen in figure 6. At the centreline, from these results, the turbulence Reynolds number based on the integral scale was calculated to be about 150, the integral scale to be 11 mm, the Taylor scale 3.5 mm and the Kolmogorov scale 0.26 mm. Corresponding values at measurement points for other conditions are given along with these in table 1.

Measurements are reported for the centreline and off-axis positions A and B shown in figure 7 and given in Table 1. Figure 7 is a plot of contours of constant values of the average measured ion current to an EP sensor in the flame of equivalence ratio 1.10. Point A is the position of maximum average ion current on the centreline. Point B, assigned a vertical height z half that of point A, is located at the radial, r, position where the average ion current is maximum. The average ion current at point B exceeds that at point A and is nearly the largest found anywhere in the turbulent flame brush. Measurements also were made at the maximum-current point at three-quarters of the centreline height in this flame; the results are very much like those at the half height and therefore are not shown here. Certain centreline measurements were also made in this flame at points above and below point A where the average ion current was half its maximum value. These results, as well as results for the flames of the two other equivalence ratios indicated in table 1, are discussed in the next section. The centreline and off-axis measurement positions at the two other equivalence ratios also coincided approximately with positions of maximum average ion current, as at points A and B, but to achieve this in these other flames, the vertical position z is larger, and the off-axis points are located at different radii r.

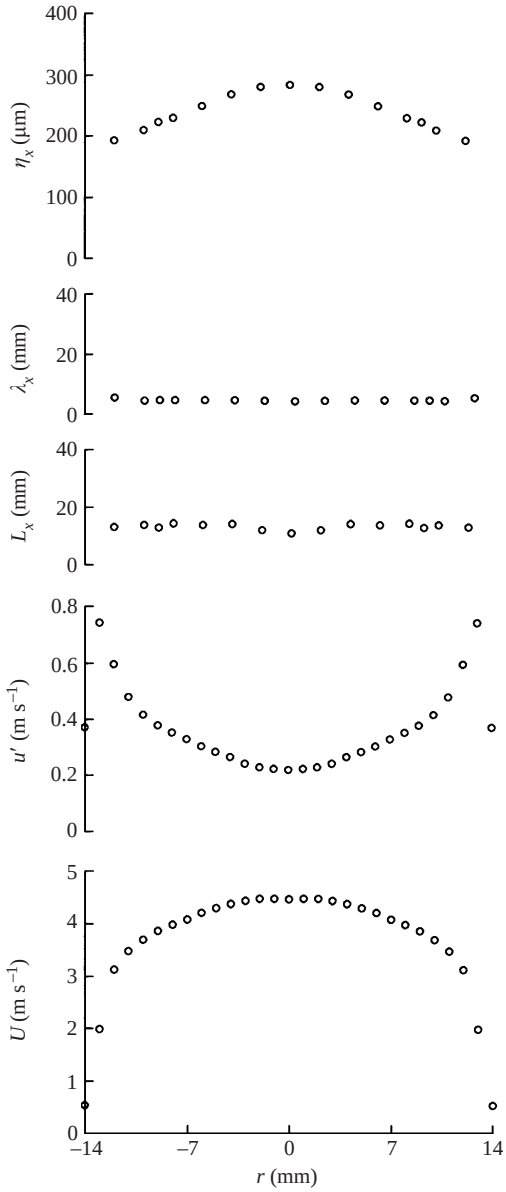

FIGURE 6. Burner-exit profiles of mean velocity U, root-mean-square velocity fluctuation u', integral scale L_x, Taylor scale λ_x and Kolmogorov scale η_x, obtained by hot-wire anemometry in cold flow.

The mixture, flow and measurement-point selections for the equivalence ratio of 1.10 were designed to maximize the accuracy and reliability of the EP data. Of all alkane–air flames, this fuel mixture has a laminar burning velocity among the highest and correspondingly a laminar flame thickness among the smallest, so as to assure that conditions lie in the flame-sheet regime, to the greatest extent possible. Differences in burning velocity are not very great for the alkanes, so the results are quite likely to be representative of other fuels as well. Rich flames of propane and higher hydrocarbons exhibit diffusive-thermal cellular instability that increases flamelet curvature (Williams 1985), but this tendency for propane is relatively small at an equivalence ratio of

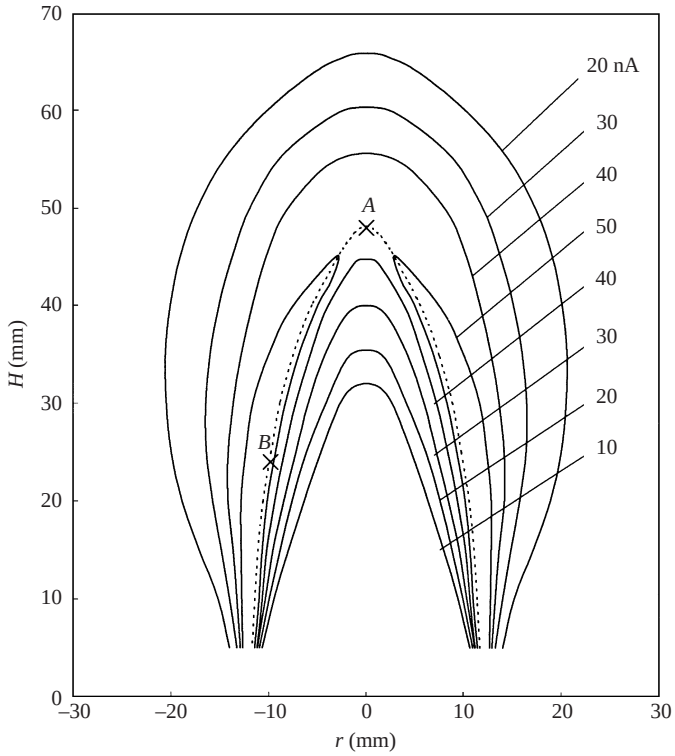

FIGURE 7. Measuring positions in the turbulent flame brush for an equivalence ratio of 1.10; ——, contours of constant values of the average ion current; – – –, the locus of the maximum average ion current as a function of height.

1.10 and becomes strong only at higher equivalence ratios. Locally planar flamelets therefore can be encountered in this mixture. Reynolds numbers are high enough for there to be a reasonable Kolmogorov subrange, facilitating interpretations. The measurement points on the contour of maximum average ion current have the maximum probability of encountering flamelets that register on all three EP sensors. The relatively large number of thin flamelets with narrow EP peaks thus optimizes the fidelity of the measurements at this point. The data at the other two equivalence ratios and at the other two average ion currents were taken to investigate possible influences of these parameters on the results.

Velocity vectors in the measurement plane for the events analysed at equivalence ratio $\phi = 1.10$ are shown in figures 8 and 9. Subscripts on the velocity V are f for flame, g for gas, r for radial, z for axial, a for ahead of the flame in the approach flow and b for behind the flame in the burnt gas. The analysis for extracting flamelet velocities and orientations from the EP data is detailed by Furukawa *et al.* (1998*a*). For the gas velocities in figure 8, blue symbols are measurements ahead of the flame and red symbols behind. Most of the velocity vectors off axis point away from the burner axis, whereas the distribution is symmetrical on the centreline. Although gas velocities in the burnt gas are seen in figure 8 to exceed those in the fresh mixture, the velocity increase is appreciably less than would occur for a planar one-dimensional flame, probably because of local flamelet orientation, flamelet movement and tangential gas-expansion effects. Flame-front velocities occasionally can be larger even than burnt-gas velocities because only the projection into the measurement plane

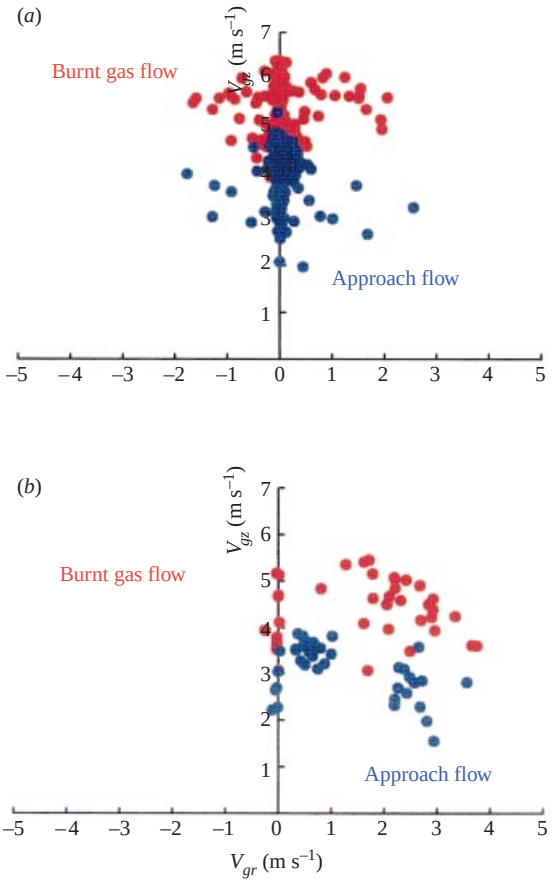

FIGURE 8. Vector distribution map of the gas velocities in the approach flow and burnt gas for an equivalence ratio of 1.10. (*a*) Centreline. (*b*) Off-axis.

is recorded; flame fronts not perpendicular to that plane and moving normal to it can register large velocities of the line of intersection.

From flame-velocity data such as those in figure 9, the probability-density functions for flamelet orientation shown in figure 10 are readily generated. The angle between the horizontal direction and the line of intersection of the flamelet sheet with the vertical measurement plane is denoted by θ_f, while N and N_s represent the number of samples in a flame-angle bin of 5° interval and the total number of samples, respectively. The anticipated symmetrical distribution is observed at the centreline, while the flamelet normal pointing towards the burnt gas tends to be directed away from the burner axis at off-axis positions, although the average angle of inclination is less than 30° even off axis. These data are of interest in modelling turbulent combustion and can be further interpreted by the methods of Zhang, Bray & Rogg (1998), who were concerned with counterflow turbulent flames, but developed approximations that can be used for the present flames as well. Similar distributions of flame angles have been measured by a different technique for rod-stabilized flames (Knaus & Gouldin 2000).

An additional relevant aspect of the results shown in figures 8–10 is that there are systematic differences depending on whether the flame passes the probe in the burnt-to-unburnt or unburnt-to-burnt direction. In the centreline data of figure 8, many points have nearly vertical velocity vectors. For most of these points, the flame

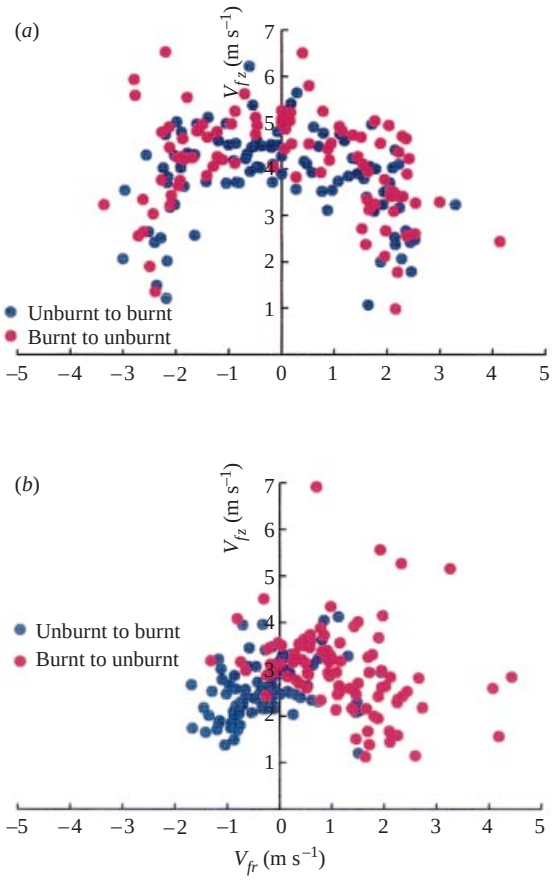

FIGURE 9. Vector distribution map of the flame-front movement for an equivalence ratio of 1.10. (*a*) Centreline. (*b*) Off-axis.

passes the probe from the burnt to the unburnt side. When the flame passes from the unburnt to the burnt side, the velocity vectors are distributed nearly uniformly over the range of directions seen, and the vertical component of the approach-flow velocity tends to be smaller, while that of the burnt-gas velocity tends to be larger, so that the vertical component of the velocity change is larger. This is consistent with the idea that nearly vertically oriented wrinkled flamelets with cusps pointing towards the burnt gas are moving upward; these flamelets pass from burnt to unburnt when velocities are predominantly vertical, whereas those that pass from unburnt to burnt do so with more of a flapping motion of the gas velocity, with fronts oriented more normal to the measurement plane, so that larger velocity changes are recorded. The flamelet velocity vectors have similar distributions for these two directions of motion in the centreline measurements of figure 9, suggesting relatively deep wrinkles, with many of the upward-moving cusps having nearly horizontal nearby flamelet surfaces.

Off-axis, on the other hand, there is little difference in the gas-velocity distributions of figure 8 for the two different directions of passage, but the flame-front velocities of figure 9 have predominantly outward radial velocities for flamelets passing the probe position from the burnt to the unburnt side but are more nearly symmetrically distributed, as on the centreline, for flamelets passing from unburnt to burnt. This indicates that off-axis positive radial velocity fluctuations are largely responsible for

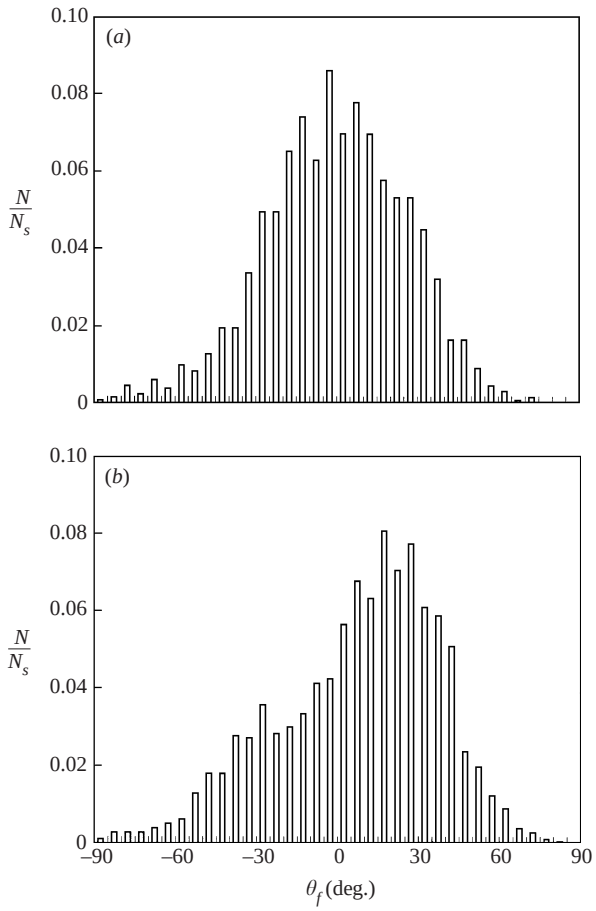

FIGURE 10. Probability distribution of flame-front orientation for an equivalence ratio of 1.10. (*a*) Centreline, $N_s = 1336$. (*b*) Off-axis, $N_s = 1770$.

flamelet passage in the former situation, whereas vertical convection of the wrinkled flamelets is more likely to cause the flamelet passage in the latter, leading to the relatively small most-probable flame angle off-axis in figure 10. These observations provide some idea of the probable flamelet geometry and motion, which may be kept in mind in subsequent considerations.

Figures 11 and 12 show representative tests of jump conditions at both positions. These vector diagrams, which have the same orientation as those of figures 8 and 9, show the normal and tangential components of gas velocity ahead of and behind the individual flamelet. The main diagrams in figures 11 and 12 show that, within the accuracy of the measurement, the tangential component of gas velocity is unchanged in crossing the flamelet, while the normal component of velocity increases, in agreement with theoretical expectations. From the data records, more than 40 such measurements were analysed at each position, and only about 10% of the vector diagrams exhibited measurable differences in the tangential velocity components ahead of and behind the flame. A diagram illustrating such a difference, representative of the average of those exhibiting differences, is shown as a small inset at the bottom left-hand side of figure 11. At the extremes, mainly for measurements showing small tangential gas velocity components, the tangential component of the gas velocity in the burnt gas

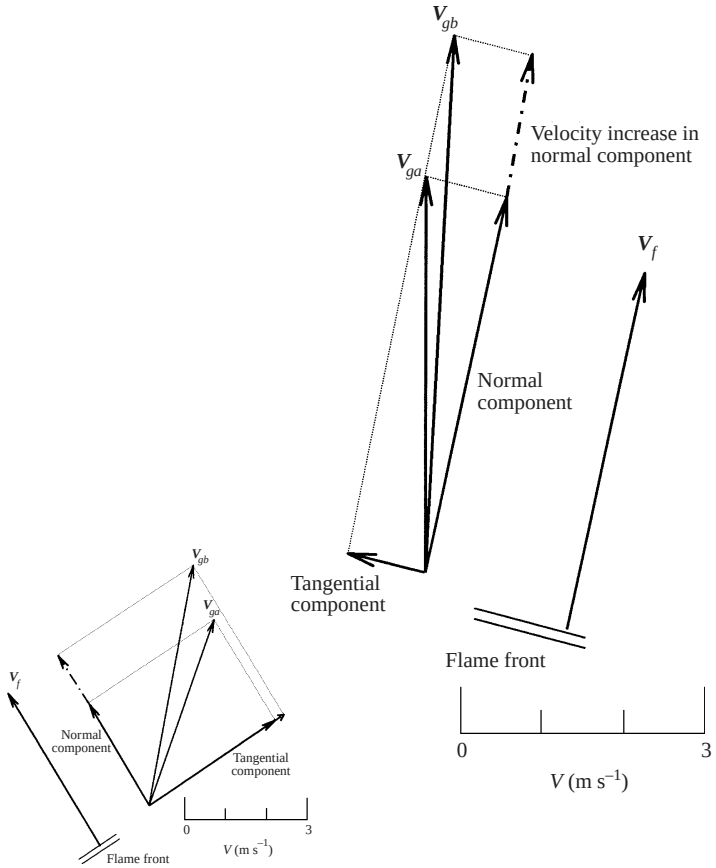

FIGURE 11. Representative change in local gas velocity vector across the flame front on the centreline.

varied from 65% to 140% of that in the unburnt mixture. These departures, well in excess of the estimated maximum 5% LDV error, may be attributed to passage by the probe of a cusp region of the flamelet. Cusps are known to occupy roughly 10% of the flamelet surface through cellular-type instabilities at propane–air equivalence ratios of 1.10, and relatively large streamline deflections occur through these flame-curvature effects, as has been seen experimentally for laminar cellular flames and demonstrated recently by direct numerical simulation (T. Hasegawa, personal communication 2001). The neglect of curvature effects, as illustrated in figure 5, thus is reasonable for only about 90% of the flamelets encountered at this equivalence ratio. The experimental method, in fact, enables velocity components to be tracked through a flamelet, giving 5 to 10 interior points and exhibiting effects of flamelet curvature and of small turbulent eddies, as continuing research is showing.

The measured increase in the normal component of gas velocity in passing through a flamelet, illustrated in figures 11 and 12, was found to be less than predicted for a steady planar flame. The maximum observed increase in the normal component was about $2\,\mathrm{m\,s^{-1}}$, less than the $2.8\,\mathrm{m\,s^{-1}}$ calculated for a stationary planar one-dimensional flame. Although part of this difference may be attributable to the flamelets not being normal to the measurement plane, so that only one component of the change in normal gas velocity is measured, the difference is so large that local gas-expansion

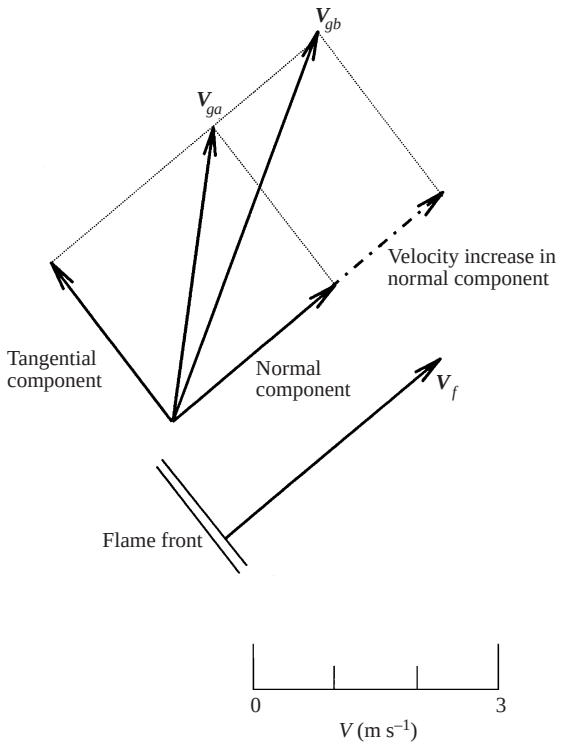

FIGURE 12. Representative change in local gas velocity vector across the flame front off-axis.

effects would seem to be important as well. Such effects can reduce the magnitude of the normal gas velocity components without altering the transverse component. The results in figures 11 and 12 thus appear to be comprehensible on the basis of considerations of turbulent flame structures.

5. Conditional spectra of turbulent kinetic energy

Since the different behaviours of the transverse and normal velocity components in crossing flamelets suggest generation of anisotropy, it is of interest to measure conditioned velocity spectra, to ascertain consequent differences in statistics in burnt and unburnt gases. Although many different types of spectrum can be considered (Lagrangian *vs.* Eulerian, space *vs.* time), the LDV is best suited to Eulerian time spectra in the present statistically stationary flows. Only one EP sensor is required for conditioning on fresh *vs.* burnt mixtures, and, in the present experiments, the sensor nearest the LDV measurement point is employed for this purpose; for the experiments other than those at points A and B of figure 7, only a single-element EP was employed. The power spectrum density function $P(f)$ is obtained as a function of the frequency f (cycles per second) from a Fourier transform of the time series of the fluctuating part of the velocity in the usual manner; that is, the average value of the product of the departure of the velocity from its mean at time t with that at time $t+\tau$ is $2\pi\int_0^\infty P(f)\cos(2\pi f\tau)\mathrm{d}f$. Mean velocities and spectra are calculated separately for radial and axial velocity components and for fresh and burnt gas at each measurement position of figure 7. Errors in mean velocities are of the order of $0.01\,\mathrm{m\,s^{-1}}$ in cold flow and less than $0.20\,\mathrm{m\,s^{-1}}$ in hot flow. Results of these

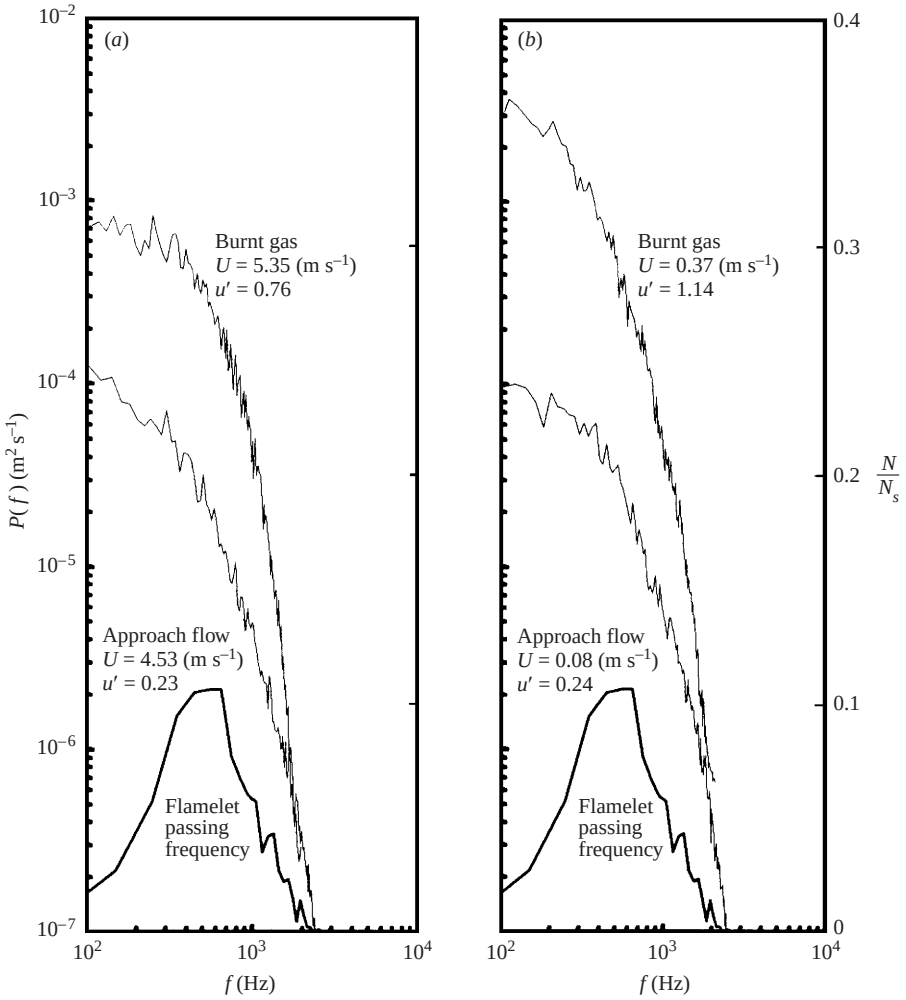

FIGURE 13. Change of the power-spectrum density function across the flame front on the centreline for an equivalence ratio of 1.10 at the position (A of figure 7) of maximum average ion current. $N_s = 855$. (a) Axial. (b) Radial.

measurements and of measurements in other flames and at other points in figure 7 are shown in figures 13–21. Also shown in these figures for use in comparisons is the probability-density function for the flamelet crossing frequency recorded by the EP, denoted by N/N_s.

The good quality of the data for $P(f)$ in these figures is a consequence of a detailed study of requirements for obtaining spectra by LDV (Furukawa *et al.* 1996). This study, which employed hot-wire measurements with variable A/D conversion as well as the LDV, demonstrated by varying the number of data processed and the conversion rate that at least 2.5×10^5 data points are required to eliminate noise and that a conversion frequency of at least 20 kHz is required to capture the entire spectrum to the Kolmogorov scale. With the LDV, there is the additional complication of the random time intervals between signals. Under the experimental conditions, at the seeding conditions employed, it was established that the LDV can detect frequencies well between about 100 Hz and 20 kHz, the limiting condition for the latter value

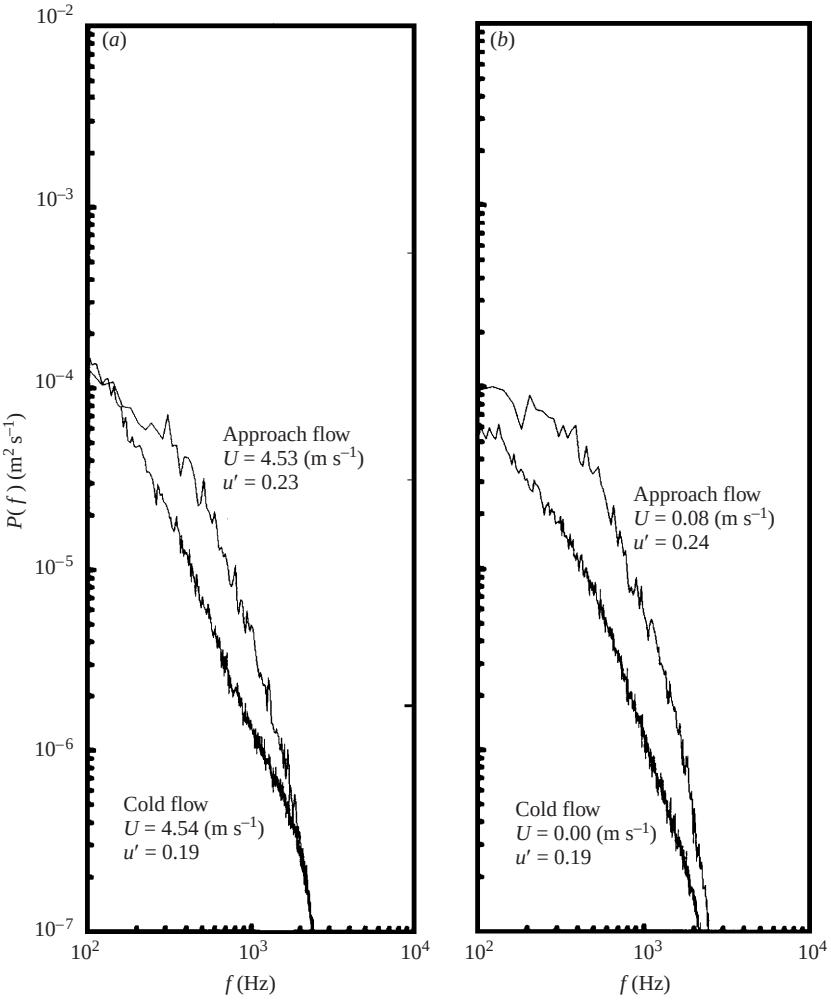

FIGURE 14. Comparison of spectra of the unburnt gas in cold flow and with the flame present at position *A* of figure 7. (*a*) Axial. (*b*) Radial.

being the seeding density in the burnt gas. The resulting spectra shown here, each based on more than 5×10^5 data points, are better than those presented previously (Furukawa *et al.* 2000, data only at point *A* in figure 7) and much smoother than those of Gökalp *et al.* (1988) or Videto & Santavicca (1990).

Interpretation of the results requires consideration of exactly what is being measured and of influences of the conditioning. At the fixed measurement point, flamelets fluctuate about the measurement position, so that the distance of the measurement point from a flamelet varies. If there is a systematic change in spectra with distance from a flamelet in either the fresh or burnt mixture, the change then will not be revealed. Instead, only a kind of distance-averaged behaviour, separately on each side of the flamelets, is represented in the results. The conditioning causes there to be periods of time during which no data on velocity are acquired for the fresh mixture, and similarly for the burnt gas. These periods must be considered in treating the data and affect the low-frequency contents of the signals. In the present work, the periods during which the conditioning eliminates data are simply excluded, and

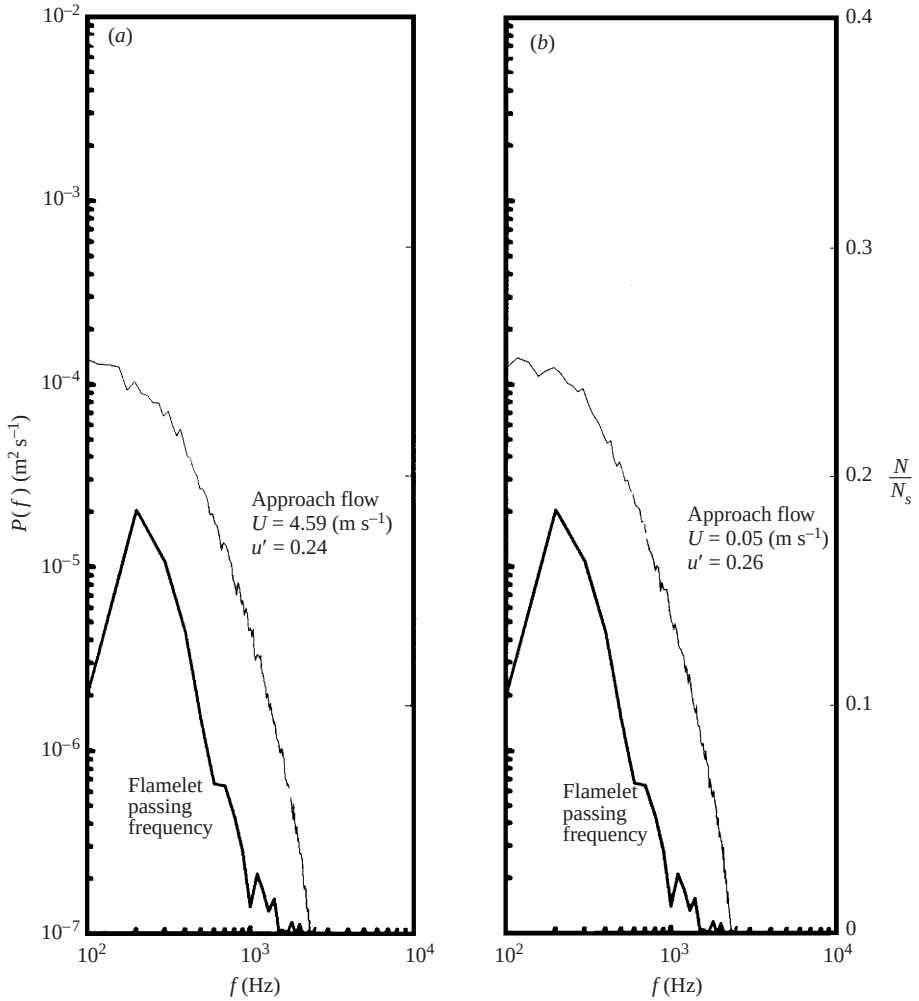

FIGURE 15. Change of the power-spectrum density function across the flame front on the centreline for an equivalence ratio of 1.10 at a position below point A where the average ion current is half the maximum value. $N_s = 1109$. (a) Axial. (b) Radial.

each data period is transformed separately by curve-fitting the data, then exercising a fast Fourier transform, and simply averaging the different resulting spectra until sufficient smoothness has been obtained. Because of the decreasing number of longer data traces, the accuracy decreases with decreasing frequency, resulting in curves that are less smooth at low frequencies in the figures. The crossing-frequency information in the figures indicates that this will not greatly affect the higher-frequency portion of the Kolmogorov subrange or measured Kolmogorov scales. Moreover, it influences all data roughly equally and therefore does not alter relative attributes of different spectral curves. Information concerning average changes in anisotropy of turbulence produced when the gas crosses the flamelets therefore can be extracted from the results with confidence. Wavelet analysis was considered as a possible replacement for Fourier analysis in treating the data, but lack of development of theory of conditioning in the context of wavelets discouraged such an approach.

It may be best first to look only at the data on flamelet crossing (passing) frequen-

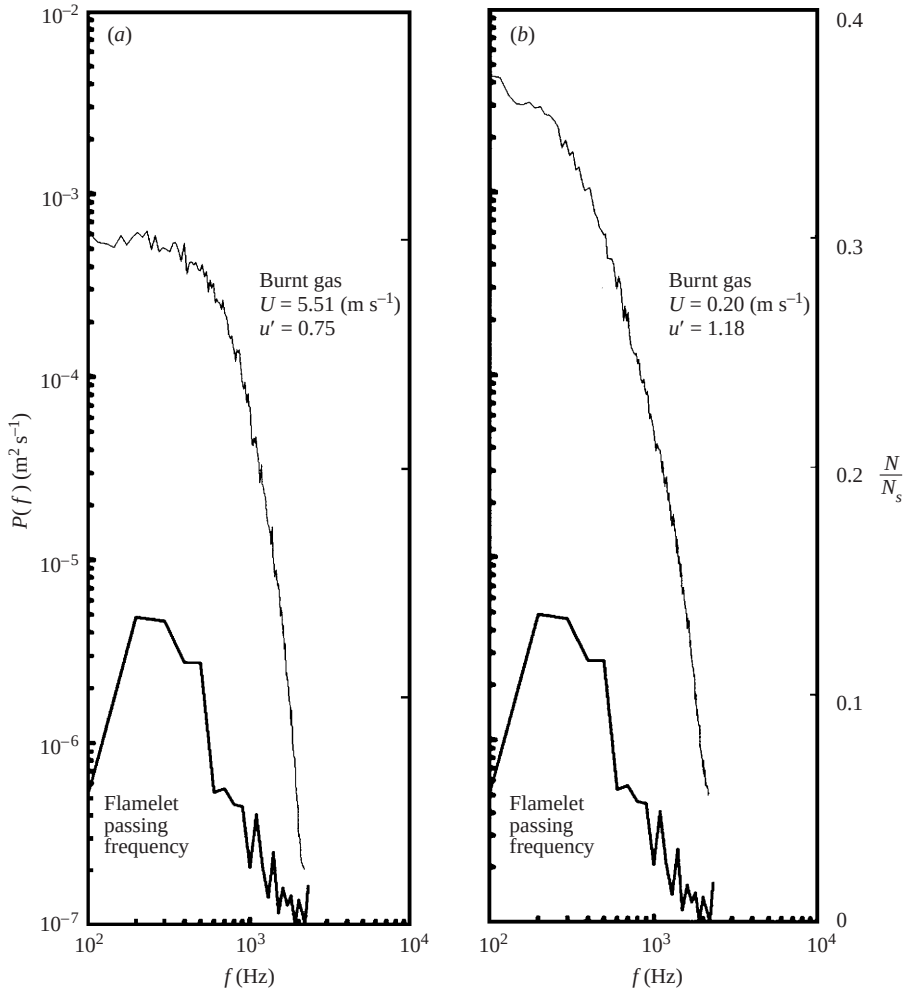

FIGURE 16. Change of the power-spectrum density function across the flame front on the centreline for an equivalence ratio of 1.10 at a position above point A where the average ion current is half the maximum value. $N_s = 1148$. (*a*) Axial. (*b*) Radial.

cies, where the notation is like that of figure 10 with a bin size of 100 Hz. Along the contour of maximum ion current, there is an observable difference in the distribution for an equivalence ratio of 0.80, compared with distributions for equivalence ratios of 1.10 and 1.40, in that the peak of the distribution is sharper at 0.80 (see, for example, figure 18). This is especially true on the centreline but also can be discerned off-axis. The difference is probably associated with the cellular structures of the flamelets. These structures are more pronounced and have smaller radii of curvature at the higher equivalence ratio and are hardly present at all for 0.80. Consequently, flamelet curvatures measured in turbulent flames are smaller at 0.80 (Furukawa *et al.* 1998*b*), and the previously mentioned complications associated with flamelet cusps are much less prevalent for this equivalence ratio. The flamelets of larger curvature may be expected to produce a broader distribution of crossing frequencies than the more nearly planar flamelets, whose distribution of crossing frequencies should drop off after the maximum more sharply in the direction of decreasing frequency because

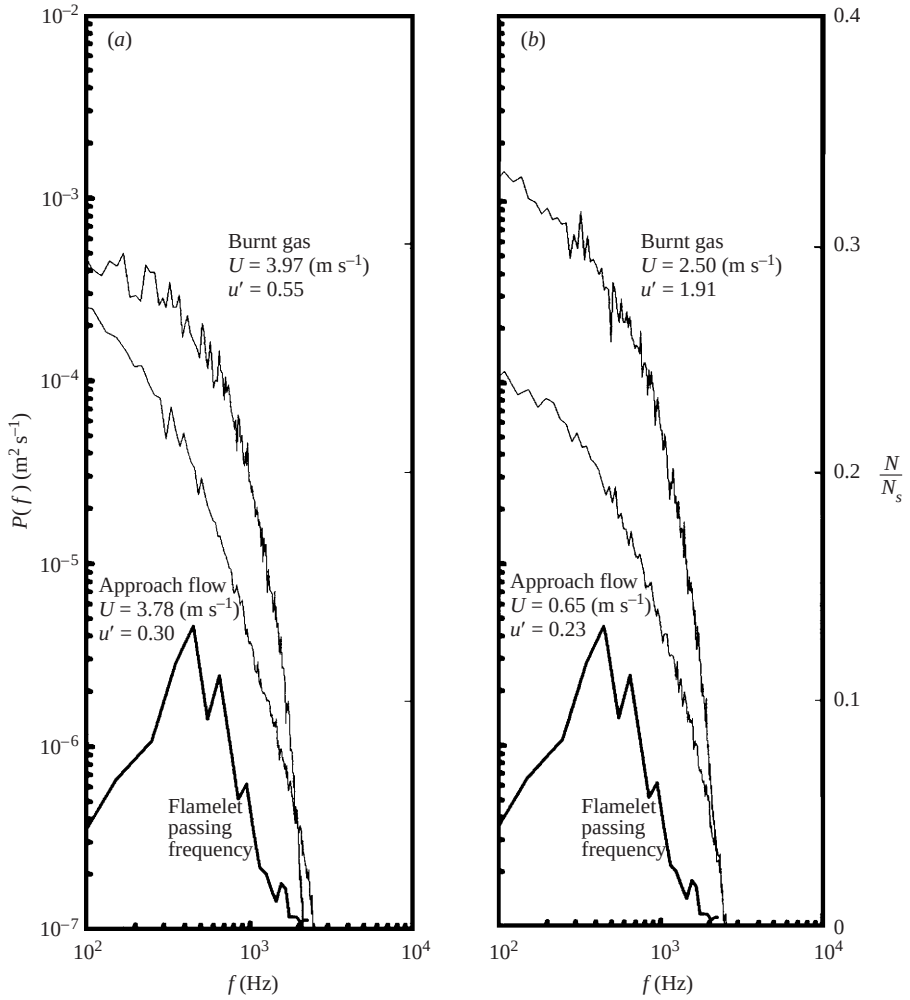

FIGURE 17. Change of the power-spectrum density function across the flame front at the off-axis position (B of figure 7) for an equivalence ratio of 1.10. $N_s = 738$. (a) Axial. (b) Radial.

of their consequent lower probability of escaping detection by not encountering the sensor. Away from the contour of maximum ion current (see figures 15 and 16), the distribution of flamelet crossing frequencies should be broader because the reduced chances of the sensor encountering a flamelet lead to relatively short periods during which the sensor is on one side for the flamelet and relatively long periods during which it is on the other side, enhancing sample-distribution contributions comparatively at large and small frequency values, away from the mean. A bimodal distribution may be expected at locations sufficiently far from the centre of the turbulent flame brush. Measurements could not readily be made at distances sufficiently large to demonstrate this because the crossing frequencies were too low. Comparison of figures 15 and 16 with figure 13 shows the decrease in the value of the peak crossing frequency at positions away from the contour of maximum ion current, associated with the less frequent flamelet arrival at positions away from the centre.

These passing-frequency effects may be kept in mind in considering the main data in figures 13–21, the conditioned spectra. The principal general observation that can

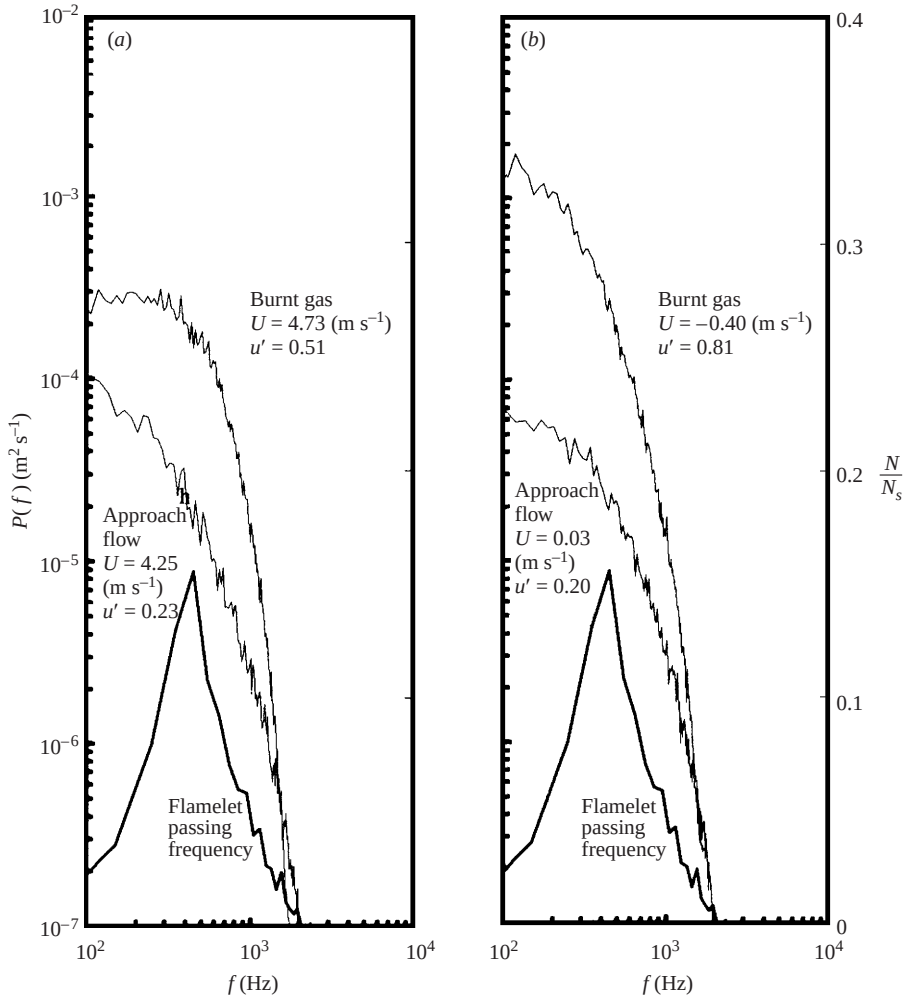

FIGURE 18. Change of the power-spectrum density function across the flame front on the centreline for an equivalence ratio of 0.80. $N_s = 751$. (*a*) Axial. (*b*) Radial.

be made from the differences in the approach-flow and burnt-gas results in all of the conditioned spectra is that the flamelets enhance the turbulence at low frequencies and reduce it at high frequencies, increasing the value of the cutoff length. Since the average component of turbulent kinetic energy per unit mass is obtained by squaring from the area under the curve (which is listed in each figure as u'), it is clear that in all cases the flamelets cause this kinetic energy to increase, that is, to be larger in the burnt gas. *In this sense, these flames exhibit the flame-generated turbulence of Karlovitz (1953).*

Another effect, entirely expected, is that through gas expansion the flame increases the average velocity. This may be seen by comparing the values of U given in figures 13–21, these values are defined as the measured conditional average velocity component, different from the burner-exit cold-flow values listed in table 1.

Another question of interest concerns the influence of the turbulent flame on the turbulence spectra. To address this question, LDV measurements were made under cold-flow conditions as well. The cold-flow measurements showed little change

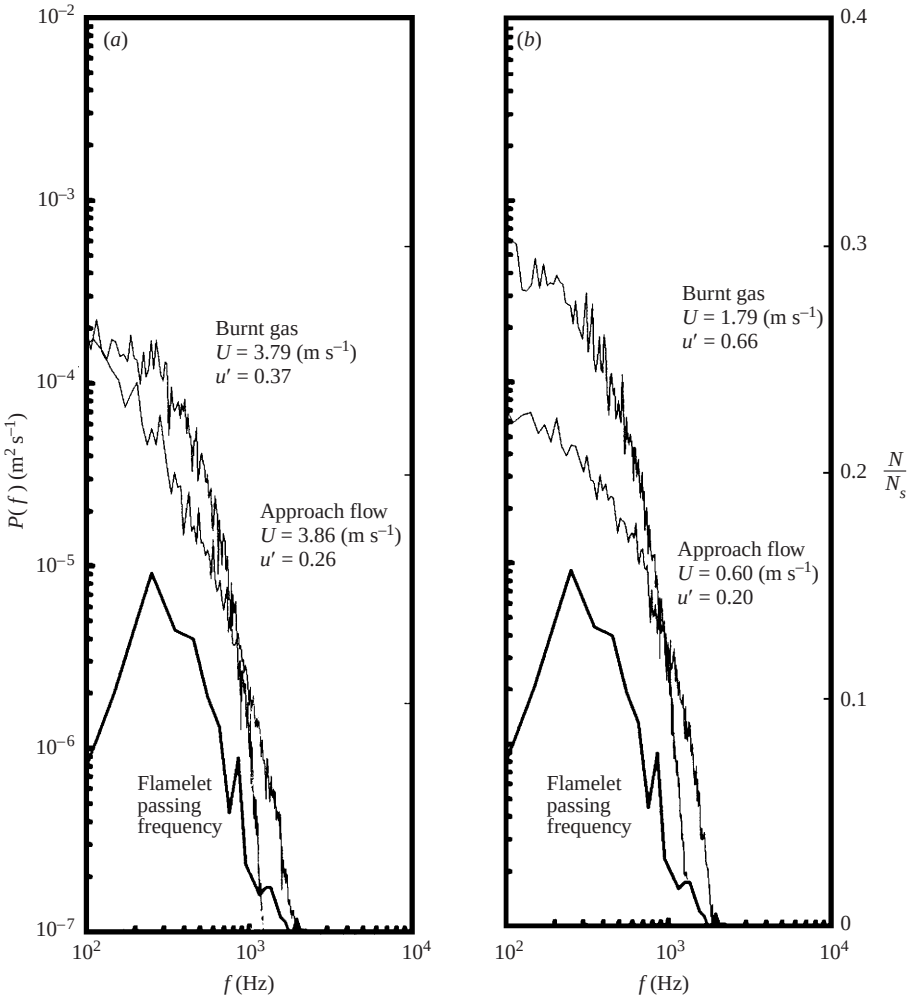

FIGURE 19. Change of the power-spectrum density function across the flame front off-axis for an equivalence ratio of 0.80. $N_s = 1038$. (*a*) Axial. (*b*) Radial.

in the spectra from just above the burner exit to beyond point *A* of figure 7, as expected. These measurements also verified the near-isotropy in cold flow, there being a tendency on the centreline (but not off-axis) for both low-frequency and high-frequency enhancement of axial fluctuations in comparison with radial fluctuations, as may be seen by comparing the two cold-flow spectra in figure 14; in view of the lower accuracy at low frequency, these differences only slightly exceed experimental uncertainity. The spectral comparisons shown in figure 14 demonstrate that, in hot flow, the presence of the flame increases the turbulence intensity in the unburnt gas at point *A*, in both axial and radial directions. This increase develops gradually in moving downstream and is less evident very near the burner exit. It may be considered to represent another kind of flame-generated turbulence, which may be peculiar to this type of burner configuration and which is weaker than that identified above.

Since the gas density is lower in the burnt gas, it is not clear from the u' results whether the total kinetic energy per unit volume (the product of the density with kinetic energy per unit mass) is increased. Use of the theoretical thermodynamic

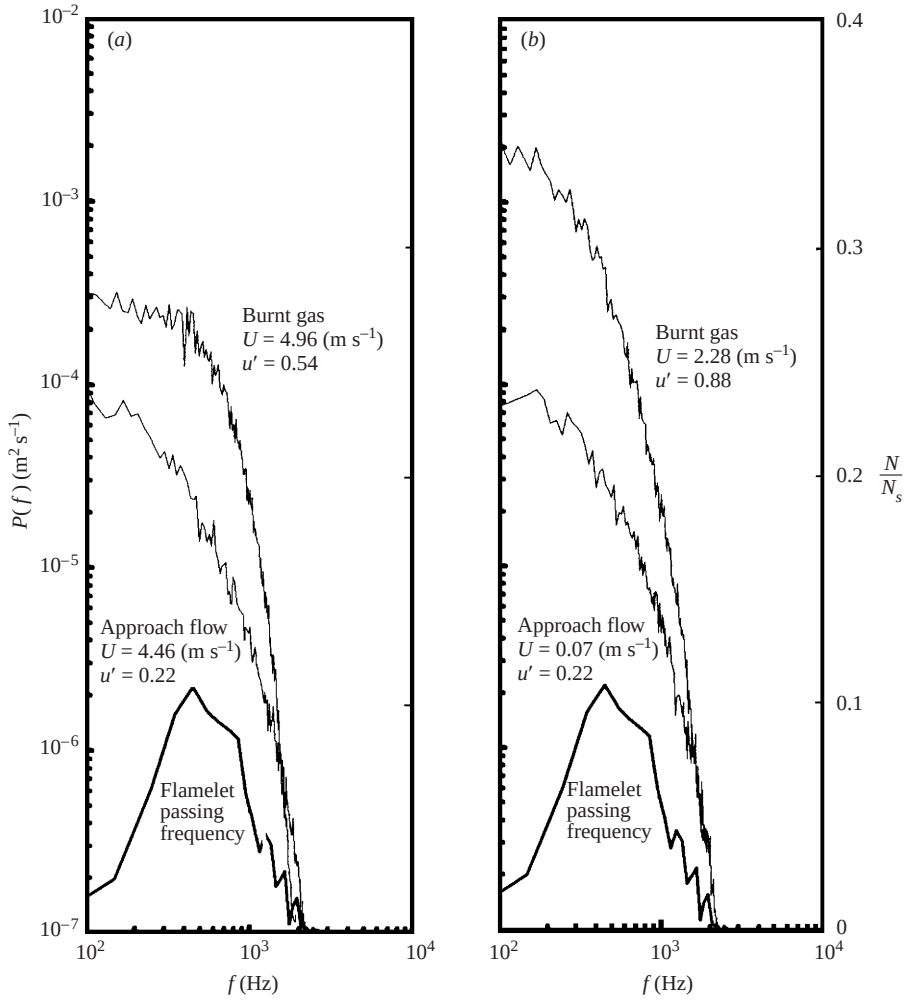

FIGURE 20. Change of the power-spectrum density function across the flame front on the centreline for an equivalence ratio of 1.40. $N_s = 844$. (*a*) Axial. (*b*) Radial.

density ratio (about 5 to 7) suggests little change in this quantity in the present data. In this respect, it is of interest to recall that for reasonable density ratios Clavin & Williams (1982) predict this quantity to increase in crossing a flamelet, whereas Aldredge & Williams (1991) show that during further traverse of the downstream hydrodynamic zone, it decreases, achieving a value typically not very different from the initial value but often somewhat lower. Comparison of the changes in the total turbulent kinetic energy per unit mass previously measured for this and other configurations, as summarized conveniently by Videto & Santavicca (1990), reveals qualitative agreement with many (but not all) earlier measurements on similar burners, although generally exhibiting a larger increase than previously observed, and there is surprisingly close agreement with the results of Videto & Santavicca, obtained in a very different configuration. On the other hand, the change is the opposite of that measured by Gökalp *et al.* (1998) for V-flames, well ahead of and well behind the average flame position. Experimental differences, in general, are attributable not so much to different measurement techniques as to measurement locations; for example,

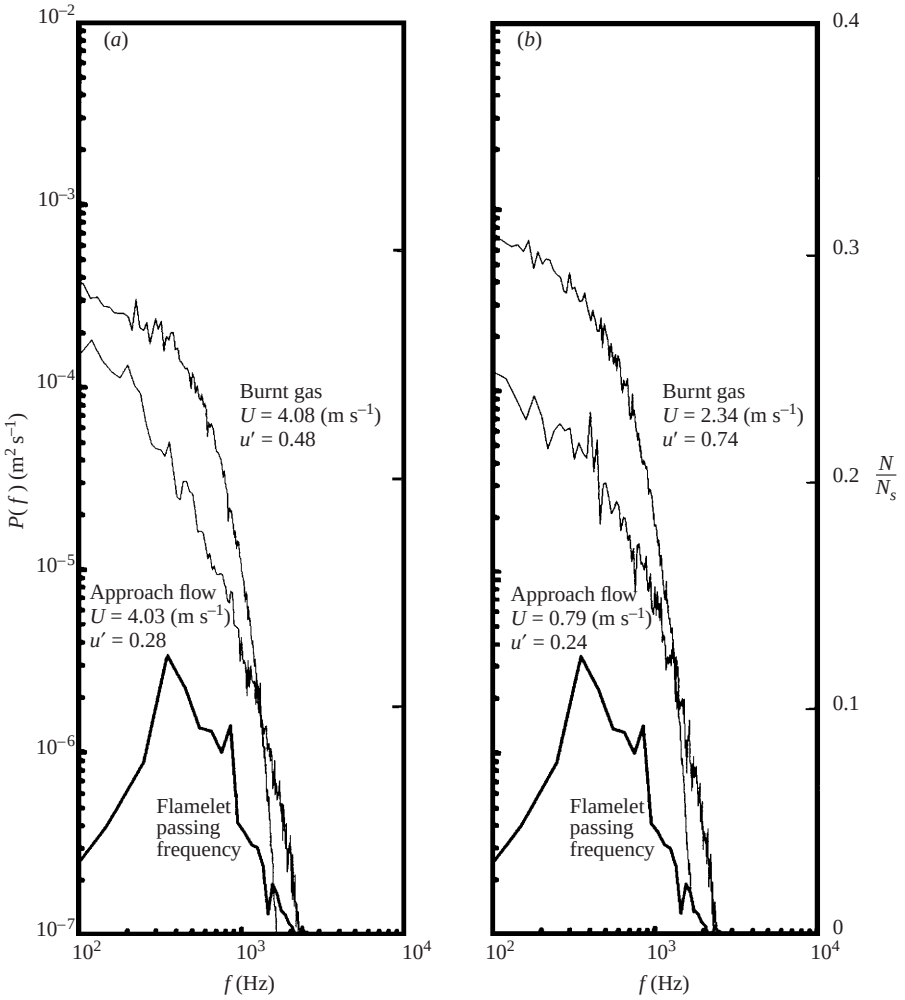

FIGURE 21. Change of the power-spectrum density function across the flame front off-axis for an equivalence ratio of 1.40. $N_s = 750$. (*a*) Axial. (*b*) Radial.

although in cold flow the decay of turbulence experimentally is negligible over the measurement distances, because of the much higher viscosity in the burnt gas, farther downstream turbulence will have decayed, contributing to the results obtained by Gökalp *et al.* (1988).

One aspect of figure 9 also has a bearing on the interpretation of the measured conditional spectra. Both on the centreline and off-axis, the measured radial components of flame velocity are both positive and negative, but the measured axial components are all positive. Off-axis, where flamelets are expected to be more nearly vertical and to propagate more nearly radially into the fluctuating fresh mixture, this might be expected as a consequence of the large average vertical convection velocity, but it could be surprising that it persists at the centreline, and the relatively small most-probable angle off-axis in figure 10 could tend to make it surprising even off-axis. If the flame at the centreline were like the flat turbulent flame considered by Aldredge & Williams (1991), then both positive and negative axial components of the flame velocity definitely would be anticipated in the laboratory frame of the

statistically stationary flame. Thus, this flame clearly is not of the assumed flat type, thereby calling into question applications of any deductions made from the theory of Aldredge & Williams (1991). Even at the centreline, then, the flame structure appears to involve fluctuating deep wrinkles, rapidly moving vertically, nearly parallel to their average surfaces, as indicated previously and as schlieren images of such flames would suggest. Off-axis, the average outward radical velocity, combined with vertical convection of wrinkled flamelets, deduced in the preceding section, affords additional ideas that bear on interpretations of the results in figures 13–21.

By contrasting figure 13 with 17, 18 with 19 and 20 with 21, it may be seen that the degree of enhancement of turbulent velocity fluctuations is generally greater on the centreline than off-axis. The approach-flow and burnt-gas spectra are closer off-axis, and the reduction in the cutoff frequency is greater there. This is consistent with the idea that in the off-axis burnt-gas measurements, on average the gas element measured has spent more time on the burnt side of the flamelet than in the centreline data. The off-axis flamelets are somewhat more vertically oriented on average (figure 10), and they tend to have a larger component of gas velocity parallel to the flamelet sheet (figures 11 and 12), so that in the off-axis data, the measured burnt-gas velocities correspond to more time having been spent in the downstream hydrodynamic adjustment zone. The intensities therefore may be lower (Aldredge & Williams 1991) than for the shorter post-flamelet burnt-gas fluid-element residence times at the centreline, although the observations made in the preceding paragraph indicate there clearly must be reservations about the strength of this inference. In addition, there may have been more time for the turbulence to decay in the high-viscosity burnt-gas fluid off-axis. These appreciable differences suggest strong sensitivities of results to precise radial measurement positions, possibly accounting for the differences in results of different investigators who made measurements on such conical burner-stabilized flames, as summarized by Videto & Santevicca (1990).

The main reason for the observed increase in the cutoff length (decrease in cutoff frequency) seems not to be rapid decay of the turbulence of the smallest scales. While it is true that the large viscosity increase across flamelets increases the rate of decay, estimates of the time available for decay to have occurred at the measurement position suggest only a small influence of decay on the results, although a larger influence off-axis, possibly contributing to the smaller cutoff frequencies there. For example, from average crossing frequencies and velocities it appears that fluid elements detected on the centreline in the burnt gas are on average perhaps 5 mm from a flamelet and have been burnt for about 2 ms, whereas a time of the order of 10 ms is required for significant decay at an eddy scale of the order of 1 mm. A tendency towards a decreased cutoff frequency is clearly detectable in the centreline data, despite the estimated unimportance of dissipation. A more probable explanation appears to be the effect of the dilatation experienced by fluid elements in crossing flamelets, which seems to be larger off-axis than at the centreline. The density decrease can increase length scales and correspondingly reduce maximum fluctuation frequencies. Although the Kolmogorov scale is larger in the burnt gas because of the higher viscosity, there is likely to have been insufficient time for equilibrium turbulence to have developed, as can be inferred from the greater departures from possible Kolmogorov scalings in the burnt-gas spectra, compared with those in the approach flow. The change in cutoff cannot be compared with earlier results of other groups because of insufficient resolution in the earlier measurements, although there is some indication of an increase in cutoff length in the data of Gökalp *et al.* (1988). On the other hand, the

increased integral scales in the burnt gas, implied by the figures, are entirely consistent with earlier experimental results.

Comparison of results in figures 13, 15 and 16 shows the influences of moving downstream in the present flames. These three points correspond roughly to positions where the average reaction progress variable is $\frac{1}{4}$ (figure 15), $\frac{1}{2}$ (figure 13) and $\frac{3}{4}$ (figure 16). Relating the average reaction progress variable to the physical positions in a precise way requires assumptions. If it is assumed that the flame thickness is infinitesimal, then the average progress variable can be obtained from Mie scattering (Cheng & Shepherd 1991) or from the average flamelet passing frequency, the spectrum of which is shown in figures 13, 15 and 16. This last definition leads approximately to the values cited above; passing-frequency profiles are similar to ion-current profiles, although there is a tendency for average ion currents to be larger on the hot side, giving progress-variable values somewhat greater than those cited. Since the average temperature in theory is linear in the average reaction progress variable, thermocouple probing was attempted as a means of measuring it, but inaccuracies and uncertainities in radiative and conductive corrections, as well as difficulties in having the thermocouples survive the flame, prevented this approach from providing better accuracy than the other methods.

Figure 15 shows only the approach-flow spectra because burnt-gas residence times were too short at this upstream position for reliable burnt-gas spectra to be obtained. Similarly, at the downstream position of figure 16, fresh-mixture residence times were too short for reliable approach-flow spectra to be obtained. Despite the lack of data, significant conclusions can be drawn by comparing the approach-flow spectra in figures 13 and 15 and the burnt-gas spectra in figures 13 and 16. The approach-flow spectra are practically identical at the two different positions, thereby demonstrating negligible changes in conditioned approach-flow turbulence properties with position along the centreline within the turbulent flame brush. Similarly, within experimental accuracy, the burnt-gas spectra are the same at the two different centreline positions. This argues against dissipation effects, associated with increased viscosity, dominating observed attributes of burnt-gas spectra and favours domination by the dilatation effect discussed above. Another conclusion that can be drawn from these comparisons is that the measured centreline conditional spectra are not strongly dependent on the location within the turbulent flame brush, but instead are approximately the same both early and late in the flame, independent of the value of the average reaction progress variable, since it can be calculated from figure 7 that the distance between each measurement point exceeds 10 mm. In general, it thus appears that the turbulent flame structure is determined by conversion of reactants to products, not by variations of turbulence properties within reactants or products.

A qualitative difference between radial and axial spectra in all cases is that the radial components of the turbulent kinetic energies in the burnt gas are larger than the axial components. In the approach flow, the radial and axial spectra and intensities are quite similar, consistent with isotropy (entirely isotropic on the centreline but slightly anisotropic, with enhanced axial intensity, off-axis), but in the burnt gas there is strong anisotropy, with fluctuations preferentially in the radial direction. Despite these reservations, this observation may be considered in the context of the prediction of Aldredge & Williams (1991) of the situation downstream in the zone of hydrodynamic adjustment and suggests that, at off-axis points, the conditions right at flamelets are not being measured on average but rather conditions somewhat downstream after hydrodynamics has been operative, consistent with the proceeding discussion. On the other hand, in the centreline measurements, conditions of the burnt-

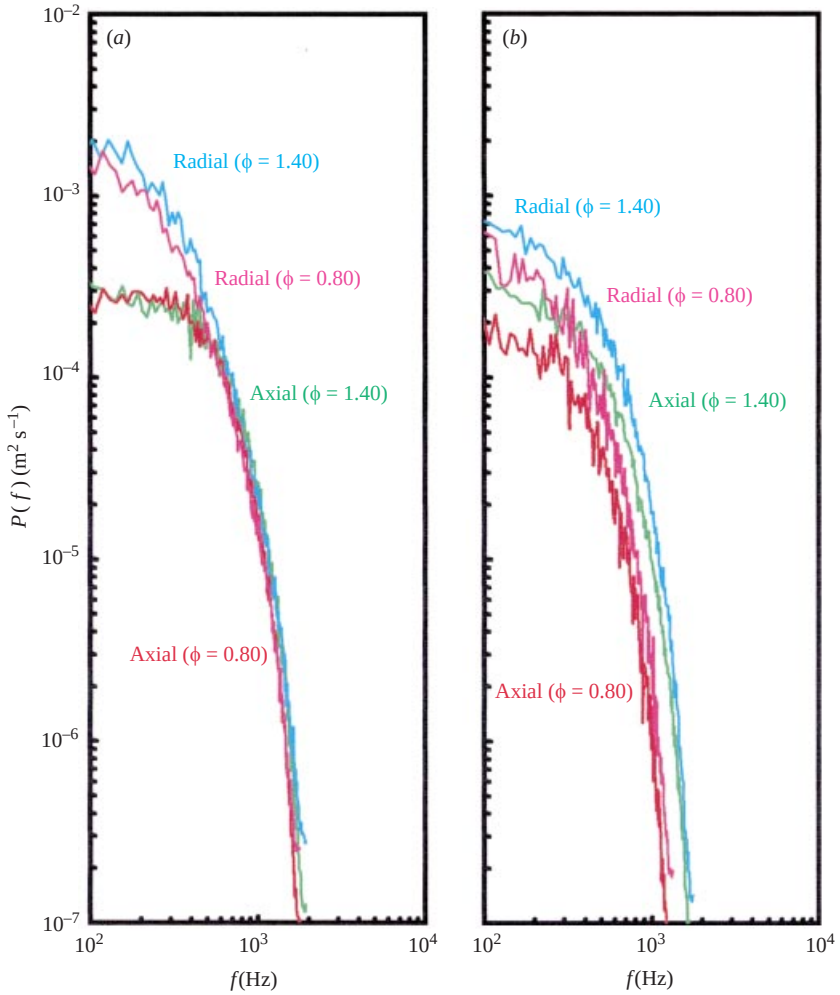

FIGURE 22. Comparisons of burnt-gas spectra for equivalence ratios of 0.80 and 1.40. (*a*) Centreline. (*b*) Off-axis.

gas measurements may be closer to the flamelets, so that the preferential transverse enhancement deduced by Clavin & Williams (1982) is observed; even off-axis, many flamelets are sufficiently horizontal that transverse enhancements would be radial (figure 10). It is noteworthy that, even in a propagating flat-flame configuration, Videto & Santavicca (1990) observed a preferential increase in the component of turbulence intensity in the normal direction, farther downstream, consistent with the results of Aldredge & Williams (1991), as might be expected, since their experimental configuration seems to be closer to that of the theory.

A further qualitative difference between axial and radial burnt-gas spectra in the figures is the tendency for a peak to develop in the vicinity of the maximum crossing frequency for the axial component but not so much for the radial component. Since it is equally prevalent on the centreline and off-axis, this aspect evidently depends more on the mean flow and not on the direction with respect to the flame normal. Review of various possible causes suggests that this effect most probably could arise from flamelets locally responding to the axial mean pressure gradient associated with

buoyancy. Estimates of magnitudes of buoyancy effects indicate that they indeed can be large enough to cause the observed modifications in the spectra under the conditions of these experiments. For example, a buoyant acceleration of $10\,\mathrm{m\,s^{-2}}$, acting over a burnt-gas resident time of 3 ms prior to the velocity measurement produces a buoyant velocity of $0.03\,\mathrm{m\,s^{-1}}$, which would not be entirely negligible in the spectrum. Since inertial effects often are assumed to dominate buoyancy in turbulent combustion, observation of this potential influence of earth's gravity on the burnt-gas conditioned spectra seems noteworthy.

It is of interest to compare the burnt-gas spectra for different equivalence ratios. Differences in approach-flow spectra and intensities are consistent with different measurement points and show relatively weak influences of the flame on the upstream turbulence; it is of greater interest therefore to focus attention on the burnt gas. The burnt-gas intensities are larger for an equivalences ratio of 1.10 (figure 13) than for equivalence ratios of 0.80 or 1.40 (figures 18 and 20); this may be expected because of the greater amount of gas expansion through the flame at the near-stoichiometric equivalence ratio. It is noteworthy that the spectra for equivalence ratios of 0.80 (figure 18) and 1.40 (figure 20) are practically identical, as may be seen clearly in figure 22; these two mixtures have the same expansion ratio and laminar burning velocity and therefore produce the same effects on the turbulence. There are differences for these two mixtures off-axis (compare figures 19 and 21 and see figure 22), where the intensities are less in the lean mixture (equivalence ratio 0.80), as might be expected from the greater degree of instability of the rich mixture, which exhibits cellular flames. The principal conclusion, however, to be drawn from the comparisons for different equivalence ratios is that the main influences of equivalence ratio arise through its effect on burning velocity and gas expansion; influences of planar-flamelet instabilities are observed only in off-axis data.

6. Conclusions and recommendations

This work, focused on structures of premixed turbulent flames in flame-sheet regimes, has confirmed that, within experimental accuracy, the steady, laminar-flame jump conditions, namely, continuity of tangential velocity components and increase in normal velocity components of a fluid in crossing a flame sheet, apply locally to individual flamelets. The increase is much less than calculated for steady planar one-dimensional laminar flames because of effects of local gas expansion in the three-dimensional turbulent field. These changes have been found to produce anisotropy of the turbulent velocity field in the burnt gas, as demonstrated by measurements of power spectra in the turbulent flame, conditioned on the presence of either a fresh or burnt mixture. In particular, there is a significant enhancement of the turbulent kinetic energy per unit mass by the flame, a kind of flame-generated turbulence. For the present flames stabilized on conical burners, the enhancement occurs most strongly in the radial direction. Flamelets produce rapid changes in power spectra leading to departures from Kolmogorov scaling and decreased cutoff frequencies, probably as a consequence of dilatation.

The work has shown that simultaneous use of laser-Doppler velocimetry with electrostatic probes can clarify a number of aspects of structures of premixed turbulent flames in flame-sheet regimes. Despite the intrusive character of the probes, which introduce interference difficulties that increase with the number of sensors, their excellent temporal and good spatial resolutions render them attractive diagnostic tools. Many different quantities have now been measured by such instrumentation, as

reported here and in cited references. Nevertheless, there is much more that can be done by these methods. For flames having locally planar flamelets, three-component velocimetry with a four-sensor probe, in principle, can provide geometrically and kinematically complete local structural information with thin flamelets, although more work would be required to reduce systematic errors of such measurements. It would be of interest to acquire additional data even with two-component, three-sensor devices of the type employed here, for example at different initial turbulence intensities and in flames of other fuels, to test the generality of the results that have been obtained and to determine whether additional phenomena occur. It would also be worth investigating the extent to which reliable measurements can be made with highly curved flamelets and in other regimes of premixed turbulent combustion. For example, electrostatic probes may well be able to identify reaction zones in the thin-reaction-zone regime; systematic testing of the range of capabilities of the devices seems warranted. In principle, entirely non-intrusive methods are more attractive, such as replacement of probes by fluorescence or Rayleigh-scattering measurements, but experimental challenges in such directions seem at least equal and perhaps considerably greater.

Since further progress in understanding of premixed turbulent combustion requires coordinated theoretical and experimental research, future testing of theoretical concepts by experiments with instrumentation such as this is an important path to progress.

Financial support of this work was provided by Grant-in-Aid for Scientific Research from the Ministry of Education, Science and Culture in Japan and the Japan Society for Promotion of Science. The authors would like to express their sincere appreciation to S. Takahashi, M. Tomosada and Y. Yoshinaga, students of Tokyo Metropolitan College of Technology, for their assistance in this work. Thanks are also extended to Mr M. Yamashita of KANOMAX Co., Ltd for his cooperation in the LDV operation. The participation of F. A. Williams was supported by the National Science Foundation through grant NSF INT9815204.

REFERENCES

Aldredge, R. C. & Williams, F. A. 1991 Influences of wrinkled premixed-flame dynamics on large-scale, low-intensity turbulent flow. *J. Fluid Mech.* **228**, 487–511.

Borghi, R. 1985 On the structure and morphology of turbulent premixed flames. *Recent Advances in Aeronautical Science* (ed. C. Bruno & C. Casci), pp. 117–138. Plenum.

Cheng, R. K. & Shepherd, I. G. 1991 The influence of burner geometry on premixed turbulent flame propagation. *Combust. Flame* **85**, 7–26.

Clavin, P. & Williams, F. A. 1982 Effects of molecular diffusion and of thermal expansion on the structure and dynamics of premixed flames in turbulent flows of large scale and low intensity. *J. Fluid Mech.* **116**, 251–282.

Damköhler, G. 1936 Einflüsse der strömung, diffusion und des wärmeüberganges auf die leistung von reaktionsöffen. *Z. Elektrochem.* **42**, 846–862.

Damköhler, G. 1940 Der einfluß der turbulenz auf die flammengeschwindigkeit in gasgemischen. *Z. Elektrochem.* **46**, 601–652.

Egolfopoulos, F. N. & Vagelopoulos, C. M. 1998 Direct experimental determination of laminar flame speeds. *Proc. Combust. Inst.* **27**, 513–519.

Fialkov, A. B. 1997 Investigations of ions in flames. *Prog. Energy Combust. Sci.* **23**, 399–527.

Furukawa, J., Harada, E. & Hirano, T. 1990 Local reaction zone thickness of a high intensity turbulent premixed flame. *Proc. Combust. Inst.* **23**, 789–794.

Furukawa, J. & Hirano, T. 1994 Fine structure of small scale and high intensity turbulent premixed flames. *Proc. Combust. Inst.* **25**, 1233–1239.

Furukawa, J., Hirano, T. & Williams, F. A. 1998*a* Burning velocities of flamelets in a turbulent premixed flame. *Combust. Flame* **113**, 487–491.

Furukawa, J., Maruta, K. & Hirano, T. 1998*b* Flame front configuration of turbulent premixed flames. *Combust. Flame* **112**, 293–301.

Furukawa, J., Maruta, K., Nakamura, T., Gomi, T. & Hirano, T. 1993*a* Fundamental study of electrostatic probe measurements to explore the structure of turbulent premixed flames. *JSME Intl J.* B **36**, 682–687.

Furukawa, J., Maruta, K., Nakamura, T. & Hirano, T. 1993*b* Local reaction zone configuration of high intensity turbulent premixed flames. *Combust. Sci. Tech.* **90**, 267–280.

Furukawa, J., Nakamura, T. & Hirano, T. 1994 Electrostatic probe measurement to explore local configuration of a high intensity turbulent premixed flames. *Combust. Sci. Tech.* **96**, 169–181.

Furukawa, J., Noguchi, Y. & Hirano, T. 2000 Investigation of flame generated turbulence in a large-scale and low-intensity turbulent premixed flame with a 3-element electrostatic probe and a 2-D LDV. *Combust. Sci. Tech.* **154**, 163–178.

Furukawa, J., Okamoto, K. & Hirano, T. 1996 Turbulence characteristics within the local reaction zone of a high intensity turbulent premixed flame. *Proc. Combust. Inst.* **26**, 405–412.

Furukawa, J., Suzuki, T., Hirano, T. & Williams, F. A. 1999 Investigation of flamelets in a turbulent premixed flame with a 4-element electrostatic probe and a 2-D LDV. *Combust. Sci. Tech.* Japanese edn, **6**, 253–262.

Gökalp, I., Shepherd, I. G. & Cheng, R. K. 1988 Spectral behavior of velocity fluctuations in premixed turbulent flames. *Combust. Flame* **71**, 313–323.

Hirano, T. 1972 An analysis of the positive-ion current to a cylinder in a weakly ionized gas. *Bull. JSME* **15**, 1402–1409.

Joulin, G. 1999 On the fractal dimension of highly-turbulent thin premixed flames. *Combust. Sci. Tech.* **141**, 107–110.

Karlovitz, B. 1953 Open turbulent flames. *Proc. Combust. Inst.* **4**, 60–67.

Karlovitz, B. 1956 Combustion waves in turbulent gases. *Combustion Processes* (ed. B. Lewis, R. N. Pease & H. S. Taylor), High Speed Aerodynamics and Jet Propulsion, vol. 2, pp. 312–364. Princeton.

Karlovitz, B., Denniston, D. W., Knapschaefer, D. H. & Wells, F. E. 1953 Studies on turbulent flames. *Proc. Combust. Inst.* **4**, 613–620.

Kerstein, A. R. 1988 Fractal dimension of turbulent premixed flames. *Combust. Sci. Tech.* **60**, 441–445.

Knaus, D. A. & Gouldin, F. C. 2000 Measurements of flamelet orientations in premixed flames with positive and negative Markstein numbers. *Proc. Combust. Inst.* **28**, 367–373.

Lam, S. H. 1964 A general theory for the flow of weakly ionized gases. *AIAA J.* **2**, 256–262.

Langmuir, I. 1923 The pressure effect and other phenomena in gaseous discharges. *J. Franklin Inst.* **196**, 751–762.

Lewis, B. & von Elbe, G. 1987 *Combustion, Flames and Explosions of Gases*, 3rd edn, pp. 226–305. Academic.

Peters, N. 1986 Laminar flamelet concepts in turbulent combustion. *Proc. Combust. Inst.* **21**, 1231–1250.

Peters, N. 1999 The turbulent burning velocity for large scale and small scale turbulence. *J. Fluid Mech.* **384**, 107–132.

Peters, N. 2000 *Turbulent Combustion*, pp. 78–127. Cambridge University Press.

Suzuki, T., Hashimoto, Y., Mashiko, I. & Hirano, T. 1979 Ion-current fluctuations recorded with a cylindrical electrostatic probe passing premixed flames. *Combust. Flame* **36**, 179–191.

Suzuki, T. & Hirano, T. 1984 Dynamic characteristics of flame fronts in a turbulent premixed flame zone. *Proc. Combust. Inst.* **20**, 437–444.

Suzuki, T., Hirano, T. & Tsuji, H. 1978 Flame front movement of a turbulent premixed flame. *Proc. Combust. Inst.* **17**, 289–297.

Suzuki, T., Kudo, N., Kawamata, M. & Hirano, T. 1986 Simultaneous measurements of gas flow and flame front movement in a turbulent premixed flame zone. *Proc. Combust. Inst.* **21**, 1385–1391.

Travers, B. E. L. & Williams, H. 1965 The use of electrical probes in flame plasmas. *Proc. Combust. Inst.* **10**, 657–672.

Ventura, J. M. P., Suzuki, T., Yule, A. J., Ralph, S. & Chigier, N. A. 1981 The investigation of time dependent flame structure by ionisation probes. *Proc. Combust. Inst.* **18**, 1543–1551.

Videto, B. D. & Santavicca, D. A. 1990 Flame-turbulence interactions in a freely-propagating premixed flame. *Combust. Sci. Tech.* **70**, 47–73.

Williams, F. A. 1985 *Combustion Theory*, 2nd edn, pp. 349–365. Addison-Wesley.

Zhang, Y., Bray, K. N. C. & Rogg, B. 1998 The modeling and measurement of local flame surface orientation in turbulent premixed flames. *Combust. Sci. Tech.* **137**, 347–358.